



Topology-Based Three-Dimensional Reconstruction of Delicate Skeletal Fossil Remains and the Quantification of Their Taphonomic Deformation

Oliver E. Demuth^{1,2,3*}, Juan Benito^{1,4}, Emanuel Tschopp^{5,6,7}, Stephan Lautenschlager⁸, Heinrich Mallison^{9,10}, Niklaus Heeb³ and Daniel J. Field^{1,11}

¹ Department of Earth Sciences, University of Cambridge, Cambridge, United Kingdom, ² Structure and Motion Laboratory, Royal Veterinary College, Hatfield, United Kingdom, ³ Department of Design, Zurich University of the Arts, Zurich, Switzerland, ⁴ Department of Biology and Biochemistry, Milner Centre for Evolution, University of Bath, Bath, United Kingdom, ⁵ Department of Biology, Universität Hamburg, Hamburg, Germany, ⁶ Division of Paleontology, American Museum of Natural History, New York, NY, United States, ⁷ GeoBioTec, NOVA School of Science and Technology, Caparica, Portugal, ⁸ School of Geography, Earth and Environmental Sciences, University of Birmingham, Birmingham, United Kingdom, ⁹ Zoological Museum, Universität Hamburg, Hamburg, Germany, ¹⁰ Palaeo3D, Rain am Lech, Germany, ¹¹ Museum of Zoology, University of Cambridge, Cambridge, United Kingdom

OPEN ACCESS

Edited by:

Matteo Belvedere,
Università degli Studi di Firenze, Italy

Reviewed by:

Michael Pittman,
The University of Hong Kong,
Hong Kong SAR, China
Marcelo Alfredo Reguero,
Argentine Antarctic Institute (IAA),
Argentina

*Correspondence:

Oliver E. Demuth
oed24@cam.ac.uk

Specialty section:

This article was submitted to
Paleontology,
a section of the journal
Frontiers in Ecology and Evolution

Received: 02 December 2021

Accepted: 31 January 2022

Published: 24 March 2022

Citation:

Demuth OE, Benito J, Tschopp E, Lautenschlager S, Mallison H, Heeb N and Field DJ (2022) Topology-Based Three-Dimensional Reconstruction of Delicate Skeletal Fossil Remains and the Quantification of Their Taphonomic Deformation. *Front. Ecol. Evol.* 10:828006. doi: 10.3389/fevo.2022.828006

Taphonomic and diagenetic processes inevitably distort the original skeletal morphology of fossil vertebrate remains. Key aspects of palaeobiological datasets may be directly impacted by such morphological deformation, such as taxonomic diagnoses and phylogenetic hypotheses, interpretations of the shape and orientation of anatomical structures, and assessments of interspecific and intraspecific variation. In order to overcome these ubiquitous challenges we present a novel reconstruction workflow combining retopology and retrodeformation, allowing the original morphology of both symmetrically and asymmetrically damaged areas of fossils to be reconstructed. As case studies, we present idealised three-dimensional reconstructions of the sternum of the crownward stem-bird *Ichthyornis dispar*, and cervical vertebrae of the diplodocid sauropod *Galeamopus pabsti*. Multiple *Ichthyornis* sterna were combined into a single, idealised composite representation through superimposition and alignment of retopologised models, and this composite was subsequently retrodeformed. The *Galeamopus* vertebrae were individually retrodeformed and symmetrised. Our workflow enabled us to quantify deformation of individual specimens with respect to our reconstructions, and to characterise global and local taphonomic deformation. Our workflow can be integrated with geometric morphometric approaches to enable quantitative morphological comparisons among multiple specimens, as well as quantitative interpolation of “mediotypes” of serially homologous elements such as missing vertebrae, haemal arches, or ribs.

Keywords: retrodeformation, 3D modelling, taphonomy, reconstruction, dinosaurs, *Ichthyornis*, *Galeamopus*, skeletal deformation

INTRODUCTION

Skeletal remains of extinct organisms allow us to trace evolutionary changes in morphology across vast timescales and provide direct insight into major phenotypic transitions throughout the evolutionary history of vertebrates (Gauthier et al., 1988; Ahlberg and Milner, 1994; Padian and Chiappe, 1998; Thewissen et al., 2001; Daeschler et al., 2006; Shubin et al., 2006; Xu et al., 2010; Hsiang et al., 2015). Unfortunately, the fossil record is incomplete and often fragmentary (e.g., Fountaine et al., 2005; Alroy, 2010; Brocklehurst et al., 2012). Moreover, taphonomic and diagenetic processes during burial and fossilisation often distort the original morphology of fossil remains, further affecting the quality of the fossil record (Benton and Harper, 2009).

Taphonomic deformation, such as plastic or brittle deformation, is often apparent in fossil remains. While such taphonomic artefacts may affect fossils of any kind, they are often particularly concerning for vertebrate palaeontologists due to limited numbers of specimens and the considerable complexity of vertebrate fossil remains. Skeletal deformation is often especially pronounced in fragile, thin-walled, and delicate specimens such as those characterised by skeletal pneumaticity [in which hollow cavities within or adjacent to bones were occupied by air-filled diverticula of the respiratory system in life (Lambertz et al., 2018)]. Fossil birds are therefore especially vulnerable to taphonomic deformation due to their relatively small size and comparatively delicate skeletons usually characterised by thin bone walls (Currey and Alexander, 1985; Brocklehurst et al., 2012). By contrast, sauropod dinosaurs were characterised by enormous size and greatly elongated necks and tails and highly pneumatized postcrania (Wedel, 2005; Cerda et al., 2012; Yates et al., 2012). However, due to their size and lightweight structure (as a result of extensive postcranial skeletal pneumaticity) (Schwarz-Wings et al., 2010), their fossil record is also generally fragmentary, and their axial bones are often similarly deformed diagenetically (Mannion and Upchurch, 2010; Tschopp et al., 2013; Cashmore et al., 2020). Although the intricate structure of pneumatic recesses, foramina, and trabecular architecture provide lightness while maintaining the strength of bones in life (Schwarz-Wings et al., 2010), these thin-walled and fragile structures are prone to breakage and distortion after an animal's death due to factors such as trampling before burial, and compaction post-burial (Benton and Harper, 2009). This distortion may hinder reasonable interpretations of detailed morphology and influence taxonomic diagnoses and phylogenetic hypotheses, as delicate structures may carry important phylogenetic information that is often

affected or entirely lost due to deformation (Bonaparte, 1999; Wilson, 1999; White, 2003; Foth and Rauhut, 2013; Tschopp et al., 2013; Kammerer et al., 2020). Additionally, functional and biomechanical analyses may lead to misleading results if plastic deformation is not appropriately accounted for (Lautenschlager, 2016). Therefore, the development of reliable retrodeformation techniques that enable the reconstruction of intricate structures without introducing additional uncertainties or inaccuracies is critical (see Tschopp et al., 2013).

Various methods have been proposed to retrodeform taphonomically distorted fossilised skeletal remains, such as rearticulation of broken fragments (e.g., Zollikofer et al., 2005; Nyakatura et al., 2015; Porro et al., 2015; Di Vincenzo et al., 2017; Wang et al., 2018), morphing reference models (Gunz et al., 2009; Vidal and Díez Díaz, 2017), and the use of landmarks (e.g., Gunz et al., 2009; Molnar et al., 2012; Tallman et al., 2014; Lautenschlager, 2016; Schlager et al., 2018; Cirilli et al., 2020). In particular, retrodeformation has been applied to bilaterally symmetrical objects, such as cranial or axial elements, as these may offer reference points from which the directionality of plastic deformation can be deduced (Ogihara et al., 2006; Arbour and Currie, 2012; Tschopp et al., 2013; Cuff and Rayfield, 2015; Nyakatura et al., 2015; Lautenschlager, 2016; Schlager et al., 2018). Thus, symmetrisation is an important step in the reconstruction of deformed palaeontological specimens, and may involve digitally restoring missing and damaged parts of a specimen and estimating the specimen's original shape (Ghosh et al., 2010; Tallman et al., 2014; Lautenschlager, 2016; Vidal and Díez Díaz, 2017). Alternative retrodeformation approaches, not employing landmarks, rely on differing assumptions and preconceived ideas about deformation processes or the response of an object to taphonomic forces during the fossilisation process. If an object is incomplete, or one side is severely crushed, the opposite side can be mirrored and superimposed to complete the missing regions (Gunz et al., 2009; Lautenschlager, 2016). However, this is only possible under the assumption that the better-preserved side is undistorted; otherwise, potential deformation artefacts will be assumed to represent genuine morphological variation, potentially introducing errors into the reconstruction.

Here, we present a novel 3D reconstruction workflow for fossilised skeletal elements based on retopology and retrodeformation. Retopology is a term originating in 3D computer animation, referring to the simplification (i.e., reducing the number of elements of a model) and re-meshing of high-resolution polygonal models (Bommes et al., 2009; Rossoni et al., 2020) into either triangular (tris) or quadrilateral surface elements (quads). In our workflow, digitised specimens are retopologised and simplified to obtain a uniformly tessellated (i.e., a regularly subdivided surface with no gaps) and topologically symmetrical mesh (for originally symmetrical objects) before they are retrodeformed. Previous work by Rahman and Lautenschlager (2017) demonstrated that such simplified surface approximations offer great potential in biomechanical analyses, such as finite element analyses (FEA), and are thus reliable alternatives to high fidelity models (e.g., see Morales-García et al., 2019; Lautenschlager et al., 2020).

Abbreviations: ALMNH, Alabama Museum of Natural History, Tuscaloosa, AL, United States; CM, Carnegie Museum of Natural History, Pittsburgh, PA, United States; FHSM, Sternberg Museum of Natural History/Fort Hays State University, Hays, KS, United States; KUVF, University of Kansas Museum of Natural History, Vertebrate Paleontology, Lawrence, KS, United States; NHMUK, Natural History Museum, London, United Kingdom; NMZ, Natural History Museum, University of Zurich, Zurich, Switzerland; PIM UZH, Paleontological Institute and Museum, University of Zurich, Zurich, Switzerland; SMA, Sauriermuseum Aathal, Aathal, Switzerland; YPM, Yale Peabody Museum of Natural History, New Haven, CT, United States.

MATERIALS AND METHODS

The three-dimensional retrodeformation method presented herein has been developed and tested on two case studies. It was first developed for and applied to several cervical vertebrae (CV) of the diplodocine sauropod *Galeamopus pabsti*, based on a single individual (SMA 0011/NMZ 1000011; Tschopp and Mateus, 2017), and further refined to reconstruct the sternum of the crownward stem-bird *Ichthyornis dispar* (Marsh, 1880; Clarke, 2004; Field et al., 2018; Benito et al., 2022). This refinement combined information from multiple individuals preserving different aspects of each bone in 2D and 3D, allowing an idealised composite reconstruction.

Galeamopus pabsti Sauriermuseum Aathal 0011/Natural History Museum University of Zurich 1000011

The cervical series was found partially articulated, with the cervicodorsal transition having been especially well preserved and in articulation (Tschopp and Mateus, 2017). The preserved cervical series consists of 13 vertebrae, which includes a complete series from the atlas to cervical vertebra 10. Three additional posterior cervical vertebrae of uncertain identity are also preserved, but these are all heavily distorted. Most cervical vertebrae were compressed transversely; however, CV 7 and 8 were predominantly compressed dorsoventrally (this deformation is most evident in the neural arch of CV 8). Neural arches in these two mid-cervical vertebrae were not fused to their centra, and were disarticulated during burial. In addition to compression, the mid and posterior cervical vertebrae were strongly sheared anteroposteriorly and dorsoventrally. These multiple aspects of deformation resulted in a complex taphonomic pattern that is not uniform along the entire cervical series. Because of this complex taphonomic history, and the extremely fragile, lightweight structure of the vertebrae, the extent of preparation was not uniform along the entire vertebral series. Cervical vertebrae 1–8 were fully mechanically prepared, whereas the posterior cervical vertebrae were only partially exposed. These were preserved in two blocks and are still partially embedded in matrix, leaving only their right sides exposed (Figure 1). Three mid-cervical vertebrae (CV 8–10) were reconstructed here. The *Galeamopus pabsti* specimen SMA 0011 (holotype) and other specimens from the Sauriermuseum Aathal (SMA) were recently donated to the University of Zurich and transferred to the collection of the new Natural History Museum of the University of Zurich (NMZ), where this specimen is accessioned under NMZ 1000011; it, however, remains on display at the SMA under permanent loan. For clarity we, therefore, refer to it using both catalogue numbers.

Ichthyornis dispar

The basis for the reconstruction and retrodeformation of the sternum of *Ichthyornis* were several 2D and 3D preserved specimens (Figure 2), described by Benito et al. (2022), showing extensive overlap and thus allowing individual well preserved

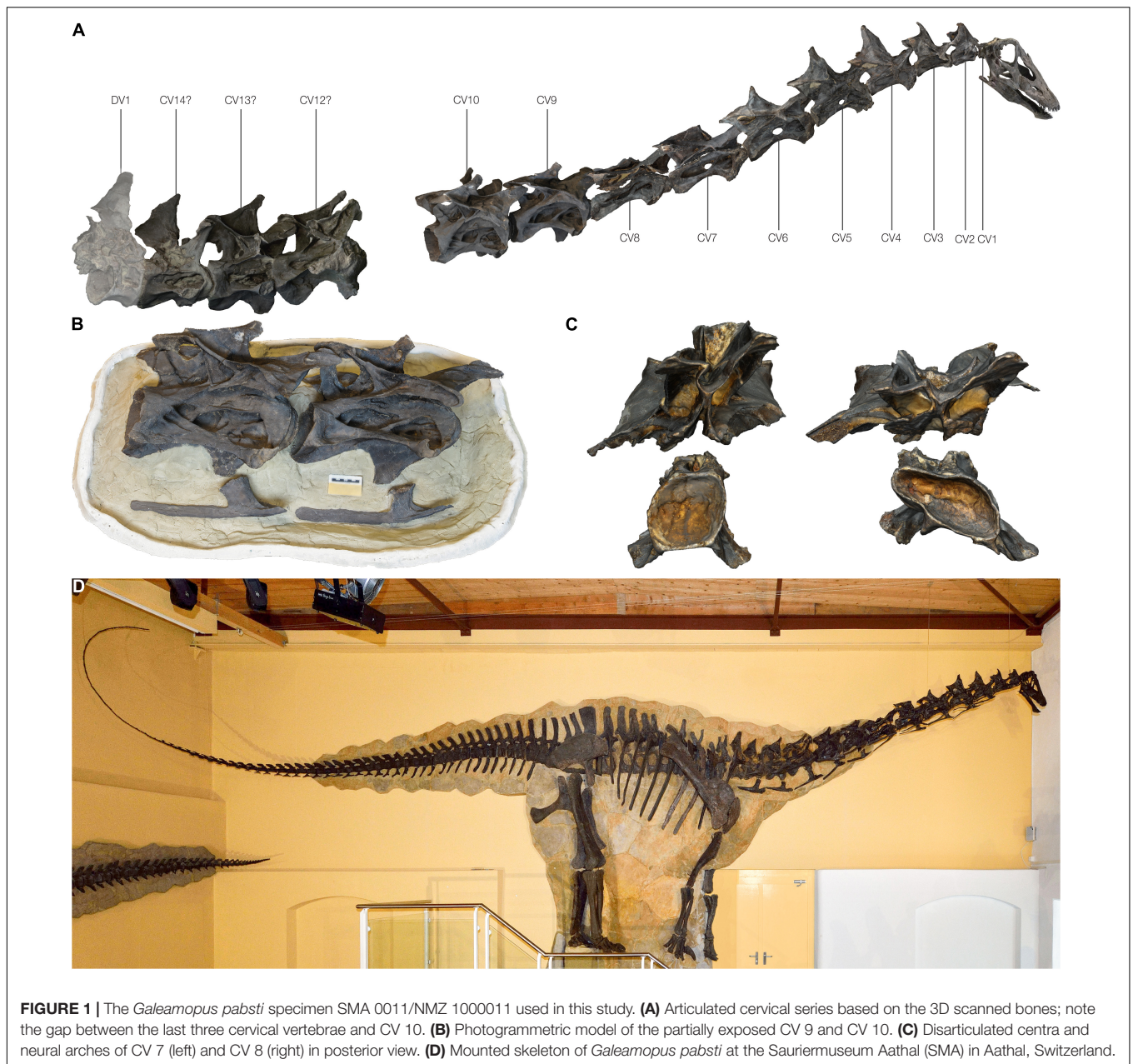
parts to be combined into an idealised composite reconstruction, hereafter referred to as a “prototype”; see Table 1. The terminology describing the preservation of the sterna follows Baumel and Witmer (1993) and Livezey and Zusi (2006).

Sternberg Museum of Natural History/Fort Hays State University VP-18702

The sternum of FHSM VP-18702 is almost complete with the anterior portion relatively well preserved, mostly in three dimensions (Figure 2A). The left side of the sternal rostrum, anterior edge of the sternal keel and the overlapping section of the coracoid sulci are particularly well preserved in 3D. The left coracoid sulcus is preserved in its entirety, although its posterior part is broken in multiple places and slightly displaced medially. The left ventral lip is crushed and distorted with a fracture extending anteromedially through it. The left craniolateral process and rib facets are folded slightly medially along this fracture. Overall, the left side of the sternum is crushed and folded with large parts overlapping each other. The elements of the right side of the sternum are generally not displaced; however, they are heavily flattened. There is a fracture along the junction of the right lateral plate with the carina extending toward the anterior coracoid pillar. Along this fracture the right side is folded dorsomedially. The right coracoid sulcus is partially preserved with the portion close to the sternal rostrum badly crushed and collapsed onto itself, exposing the internal pneumatic structure of the sternum. The posterior part of the coracoid sulcus is broken off just before the ventral lip and is shifted medially. The right craniolateral process is mostly missing. The posterior margin of the right side, including the caudolateral process and the intermediate trabecula, is well preserved. The pneumatic foramen on the anterior dorsal surface of the sternum is not discernible among the crushed and broken bone fragments in this area, but the pneumatic cavity is visible in cross-section. The general shape of the keel is well preserved although slightly mediolaterally flattened.

University of Kansas Museum of Natural History, Vertebrate Paleontology 119673

The sternum of KUVVP 119673 preserves the keel, the left lateral plate, and a part of the posterior portion of the right lateral plate (between the median trabecula and intermediate trabecula) (Figure 2B). The remaining portion of the right lateral plate is lost. The sternum is dorsoventrally flattened and, in contrast to the other two sterna discussed here, the keel is not folded laterally but is preserved in its original position, although somewhat flattened and apparently sheared. The anterior edge of the sternal keel and the sternal rostrum with the overlapping section of the coracoid sulci are extremely crushed and flattened, making it impossible to make any relevant morphological observations. The left coracoid sulcus is poorly preserved and the ventral lip is somewhat crushed and flattened. The anterior dorsal surface of the lateral plate is relatively well preserved; however, the margin is somewhat eroded and incomplete. The left lateral margin with the costal facets is completely preserved with only minor deformation and the craniolateral process appears mostly

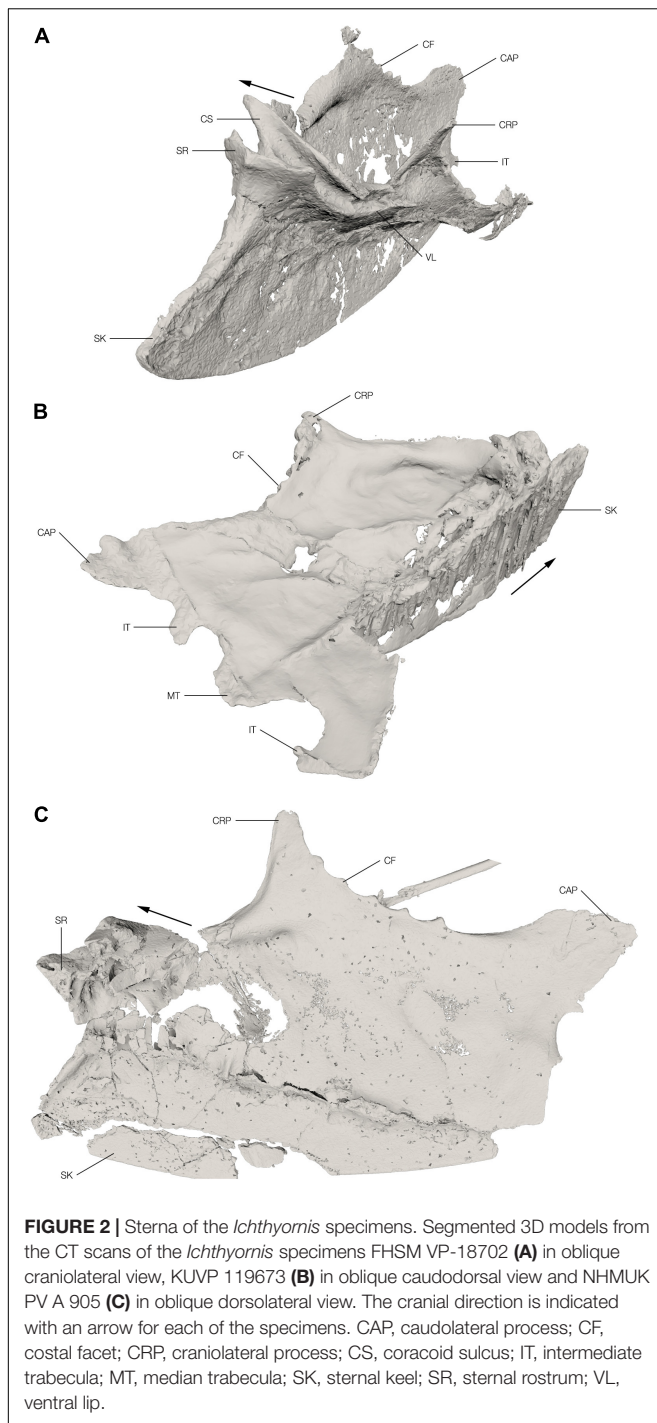


complete; however, due to radio-opaque inclusions in this area it is impossible to discern the actual extent of the preserved process. The left lateral plate has several cracks in the regions where it became slightly folded taphonomically, and a large dorsoventrally oriented hole punctured the lateral plate. The posterior margin, including the median trabecula and both intermediate trabeculae, is well preserved; however, the right trabecula appears to be deformed, thus the shapes of the left and right trabeculae do not precisely match.

Natural History Museum United Kingdom PV A 905

Only the keel and the right lateral plate of the sternum of NHMUK PV A 905 are preserved with the left side entirely

absent (**Figure 2C**). Although the element is generally flattened, a few regions are well preserved in 3D, particularly the right lateral margin, including the craniolateral process and the costal facets, as well as the posterior part of the right coracoid sulcus including the ventral lip. The right side of the sternal rostrum and most of the anterior part of the right coracoid sulcus are also preserved in 3D with minimal distortion. The dorsal margin, however, is crushed, and fragments are displaced laterally. The dorsal surface of the sternum in this area is heavily crushed and fragmented and the internal trabecular structure of the pneumatic recess is exposed. The right margin of the pneumatic foramen is well preserved; however, its exact size, shape, and position are not discernible as the fragments



are displaced. The right posterior margin of the sternum is incomplete and only the caudolateral process, the anterior margin of the lateral incisure and the base of the intermediate trabecula are preserved, while the medial incisure and the median trabecula are missing. The posterior-most part of the keel and the sternal apex are missing. A large piece of the keel is also broken off and slightly displaced ventrally; otherwise, the keel is well preserved.

METHODS

Our proposed workflow for reconstructing the undistorted morphology of a taphonomically deformed fossilised skeletal element consists of several individual steps, and varies depending on the predominant type of taphonomic deformation being addressed. These steps fall into four categories: digitisation, retopology (including repair of minor taphonomic alterations), retrodeformation, and symmetrisation (**Figure 3**).

Digitisation

Specimens were first digitised to obtain the three-dimensional morphology of the preserved elements. For our datasets we used Photogrammetry and micro-CT scanning; however, other methodologies may also be applicable (see Cunningham et al., 2014; Davies et al., 2017; Díez Díaz et al., 2021).

Galeamopus

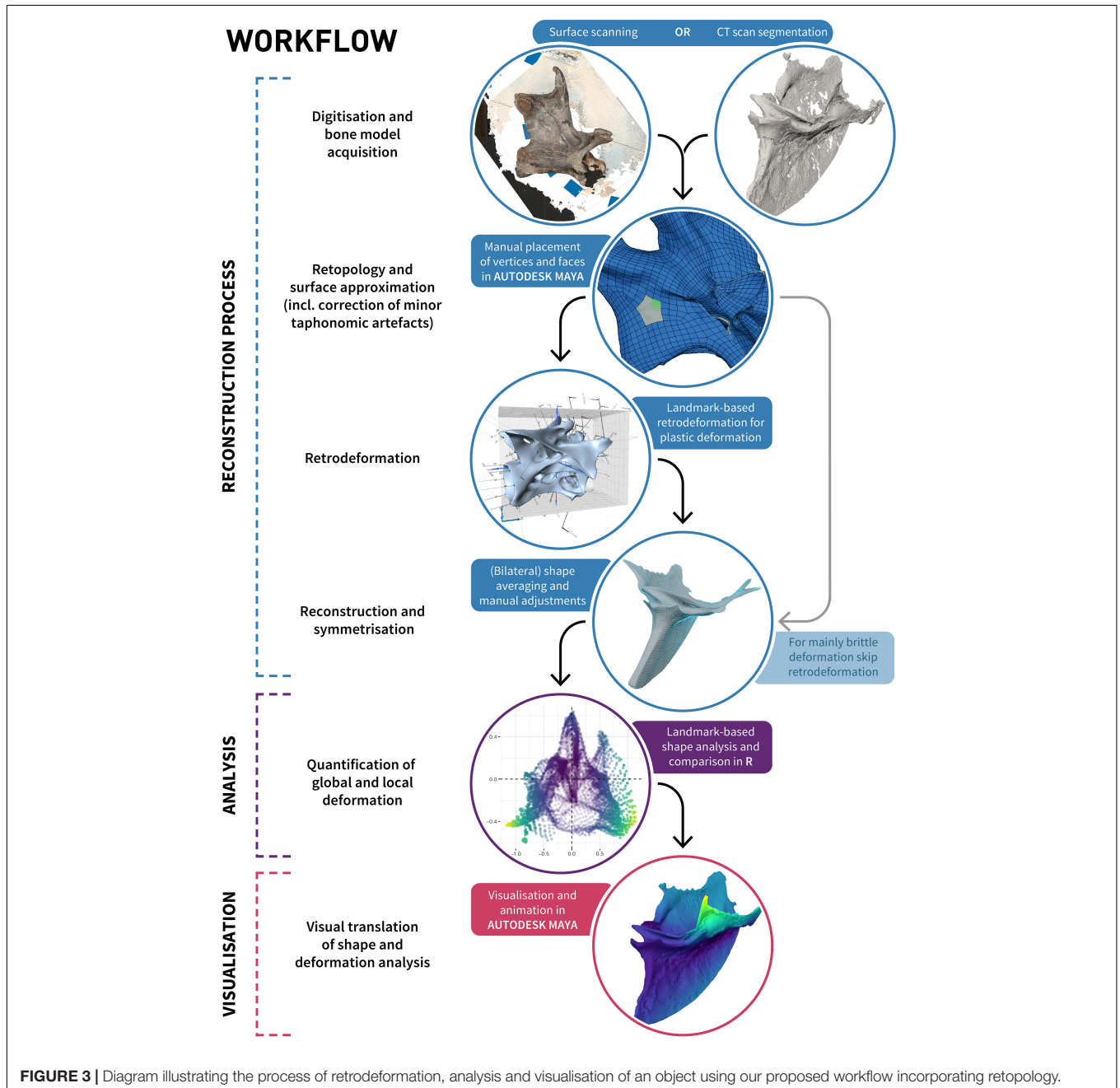
All 13 preserved cervical vertebrae of SMA 0011/NMZ 100011 were digitised individually prior to mounting of the specimen (**Figure 1D**) using photogrammetry with the software package AGISOFT PHOTOSCAN 1.3.1 (Agisoft LLC, St. Petersburg, Russia), following the approach outlined by Mallison and Wings (2014). We used a Nikon D40 with the lens AF-S DX Zoom-Nikkor 18–55 mm for initial photography. Focal length was fixed at 35 mm to minimise distortion, and ISO was set to 400 or 800, with an f-stop of 16–20, where possible. Pictures were taken with the highest available resolution in JPEG format (see also Mallison and Wings, 2014). Disarticulated neural spines and centra of CV 7 and CV 8 (**Figure 1C**) were photographed and modelled individually and reassembled in AUTODESK MAYA 1.3.1 (Autodesk, San Rafael, CA, United States). Since the posterior cervical vertebrae were only partially freed from matrix, only their exposed right side could be digitised. All digitised bones of *Galeamopus* and all resulting processing steps are available on MorphoSource (see **Supplementary Table 1** for the complete list of elements and links), following the recommendations of Davies et al. (2017) and Díez Díaz et al. (2021).

Ichthyornis

High-resolution micro-CT scans of several *Ichthyornis* sterna were obtained from multiple facilities in the United Kingdom and United States. NHMUK PV A 905 was μ CT scanned at the Cambridge Biotomography Centre, Cambridge, United Kingdom, using a Nikon 49 Metrology XT H 225 ST scanner and KUVV 119673 and FHSM VP-18702 were scanned at the University of Texas High-Resolution X-ray CT Facility (UTCT), Austin, TX, United States, see **Supplementary Table 2** for scan parameters. μ CT data were processed and the bones segmented in VGSTUDIO MAX 3.2.5 (Volume Graphics GmbH, Heidelberg, Germany). The digitised sterna of the *Ichthyornis* specimens and all resulting processing steps are available on MorphoSource (see **Supplementary Table 1** for the complete list of elements and links), following the recommendations of Davies et al. (2017) and Díez Díaz et al. (2021).

TABLE 1 | Definition of technical terms.

Term	Explanation
Prototype	Hypothetical surface approximation and reconstruction of a specimen
Mediotype	Three-dimensional interpolation of two or more surface approximations, which may be reconstructions, i.e., prototypes, but do not need to be. Not to be confused with mediotypes as defined by Belvedere et al. (2018).



Retopology

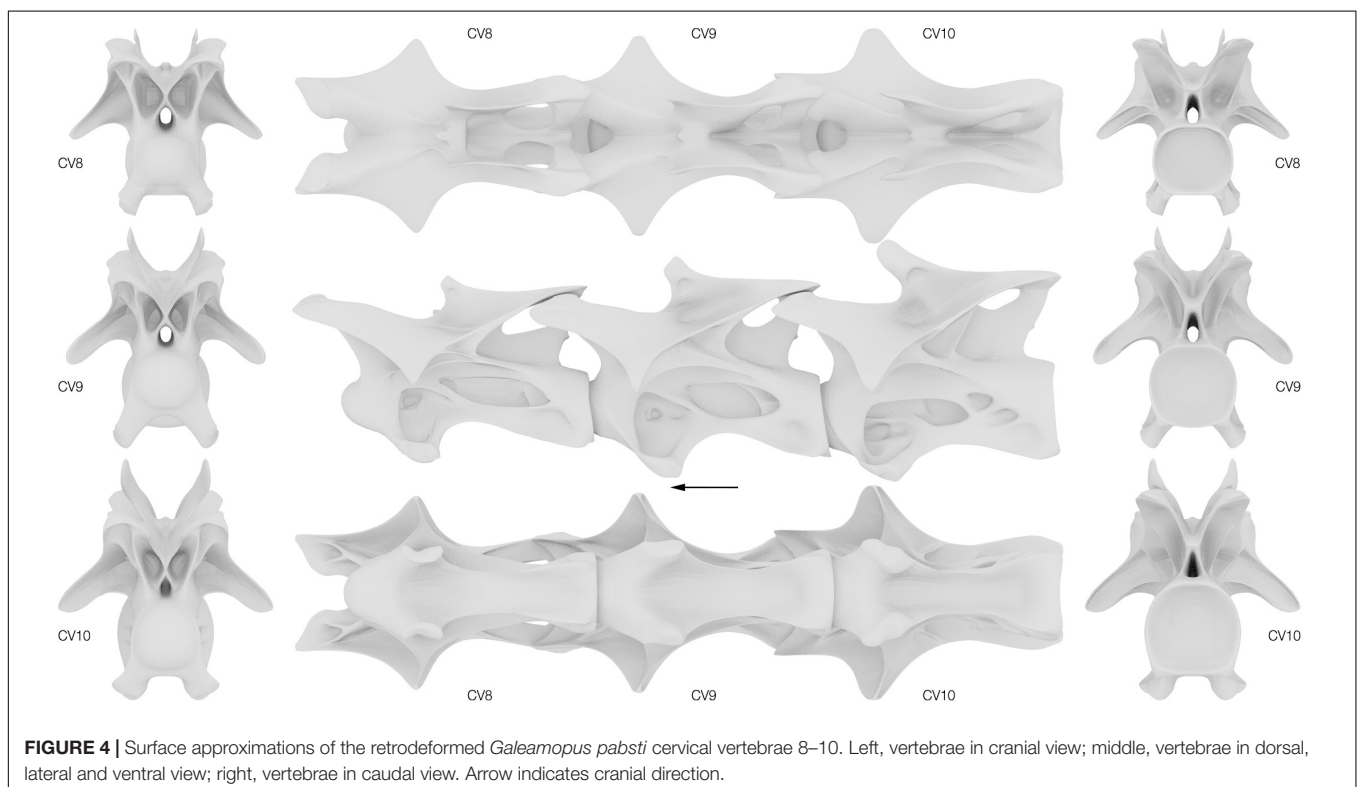
The goal of using retopology for the purpose of fossil reconstruction is to create a clean and uniform topology of a mesh approximating the shape of the preserved object. Quadrilateral tessellated surfaces (i.e., elements) are preferable

over triangular surfaces as they are more intuitive to manipulate, their representation as mostly rows and columns allows simpler subdivision and texturing (e.g., for visualisation purposes), and they are better suited for FEA and online science communication (e.g., Rahman et al., 2012; Bommès et al., 2013;

Lautenschlager and Rücklin, 2014; Rossoni et al., 2020). A quadrangular retopologised mesh represents a surface approximation of the original shape consisting solely of quads, where edges are ideally aligned with surface structures of the object, such as creases or ridges. The definition of these orientation and/or alignment constraints can either be specified manually (i.e., manual retopology), or heuristically estimated (Bommes et al., 2009). Although automated retopology is fast and a necessary step to prepare reality-based models (that is, models derived through surface digitisation techniques or CT-scanning; Cunningham et al., 2014; Davies et al., 2017; Díez Díaz et al., 2021) for analyses such as FEA (see Rossoni et al., 2020), it often lacks the control necessary to allow for further object-to-object comparisons (see below). Manual retopology provides such control and allows taking the original undistorted (*in vivo*) shape into account, with edges ideally aligned to the initial surface structure. If an object was bilaterally symmetrical in life, the topology should acknowledge its original symmetry even though the shape of the object as preserved might no longer be symmetrical. Each individual vertex should receive a mirrored corresponding vertex on the other side of the object's original plane of symmetry, thereby establishing a homologous point pair. Point pairs should be established even when the corresponding point was displaced due to brittle or plastic deformation (unless it was lost through fragmentation of the specimen or it cannot be confidently identified, e.g., if one side is still covered by matrix). The targeted and purposeful placement of vertices enables numerous downstream inferences, such as quantitative morphological comparisons among multiple specimens, as

these can be integrated into geometric morphometric analyses by treating individual vertices as landmarks. This facilitates the quantification of deformation and direct interpolations of “mediotypes” (see **Table 1**) of axial elements, which could be useful in the case of missing vertebrae, haemal arches, or ribs to fill in gaps in a skeleton (Lautenschlager, 2016). Additionally, this approach allows parts of multiple specimens to be combined into a single, idealised “prototype” (see **Table 1**), similar to the *Target Deformation* technique (Cirilli et al., 2020). Areas that are differentially preserved in multiple specimens can be combined into a single composite based on the superimposition (Lautenschlager, 2016) and averaging and/or alignment of respective overlapping vertices. As in other techniques for reconstruction and retrodeformation (e.g., Lautenschlager, 2016) or surface approximation (e.g., Rahman and Lautenschlager, 2017), minor imperfections such as cracks in a fossil can be directly addressed and removed. The general workflow is similar to the non-uniform R B-splines (NURBS)-based approach of Molnar et al. (2012); however, due to the use of polygonal modelling instead of NURBS modelling, finer control over the resulting mesh surface is possible (Demuth et al., 2022).

To retopologise digitised specimens, the high-resolution meshes were converted into a “live surface” (Molnar et al., 2012; Demuth et al., 2022) in MAYA, which allowed individual vertices to be placed directly onto the surface of the specimens (**Figure 3**; Demuth et al., 2022) using the *Modelling Toolkit*, in a manner similar to the placement of anatomically defined landmarks and semilandmarks (Bardua et al., 2019). Most individual vertices were placed manually or through subdividing



already-defined quads, and their positions were iteratively refined through spline relaxation of the vertices on the mesh surface in a manner similar to Laplacian smoothing (e.g., see Sorkine et al., 2004; Gunz et al., 2005). Vertices were placed in a targeted way incorporating bilateral symmetry only (*Galeamopus*), and bilateral symmetry and all other specimens (*Ichthyornis*) to ensure that each vertex received corresponding vertices on the other side, and the other specimens, respectively.

Bones were thus retopologised into a quadrilateral tessellated surface and thus simplified to obtain a uniform and topologically symmetrical mesh and surface approximation for both *Galeamopus* and all *Ichthyornis* specimens. Minor taphonomic alterations, such as cracks and smaller holes, were also removed during this process.

Retrodeformation

The simplest type of deformation is homogenous and unilateral compression, which can be counteracted through unilateral scaling (i.e., stretching along the deformation axis; Motani, 1997; Zollikofer et al., 2005; Di Vincenzo et al., 2017). However, this approach may be problematic as a multitude of possible stretching directions can produce a perfectly symmetrical object for any given set of homologous bilateral point pairs, precluding a unique solution for each case (Kazhdan et al., 2009). It is therefore necessary to find the optimal solution that results in minimal deviation from symmetry when uniform and unilateral stretch is applied, through additional criteria such as the minimal required stretch (Zollikofer et al., 2005; Tallman et al., 2014) or comparison with known reference shapes (Nyakatura et al., 2015). For crania, an additional point of reference is the often-circular shape of the orbit in

extant taxa, which can serve as a proxy for measuring the deviation, and therefore degree of deformation, of fossilised cranial remains (Arbour and Currie, 2012; Cuff and Rayfield, 2015; Nyakatura et al., 2015). In the absence of additional reference points, an originally bilaterally symmetrical specimen that experienced uniform compression perpendicular to, or along its plane of symmetry, can not be restored through stretching since the object would remain symmetrical despite its deformation, precluding attempts to determine the directionality of deformation (Tallman et al., 2014).

Other approaches for symmetrising objects include reflecting (mirroring) or averaging bilateral landmarks for uniformly sheared objects (Angielczyk and Sheets, 2007; Gunz et al., 2009; Tallman et al., 2014), or employing more sophisticated symmetrisation algorithms such as least-squares solutions for complex deformations (Mitra et al., 2006, 2007; Ogihara et al., 2006; Golovinskiy et al., 2009; Ghosh et al., 2010; Tallman et al., 2014). Although some of these solutions depend on assumptions that may be challenging to definitively account for [e.g., that the distances between landmarks have not been additionally altered due to compression, see Ogihara et al. (2006)], these approaches can overcome deformations not only limited to compression, but also additional bending by first addressing compressional deformation in local neighbourhoods (Ghosh et al., 2010; Tallman et al., 2014), and then restoring symmetry through clustering of local symmetry planes (Mitra et al., 2007) or a global least-squares optimisation of local symmetries (Ghosh et al., 2010; Tallman et al., 2014). Non-linear symmetrisation techniques usually rely on the placement of a number of corresponding point pairs [usually discrete landmarks, but see Mitra et al. (2007) for an automated process through curvature-based point pairing] to which an underlying mesh is retrodeformed to match its presumed original shape (Ponce De León and Zollikofer, 1999).

However, all landmark-based retrodeformation techniques have an ultimate flaw: fragmentation and brittle deformation in combination with plastic deformation may render some landmarks useless (Vidal and Díez Díaz, 2017) if individual reference points are entirely non-existent [but see Cirilli et al. (2020) for a solution to this problem] or difficult to estimate due to dislocation, displacement or folding of a specimen. Fully automated approaches are therefore not universally applicable to all specimens, which was the case for both our case studies (see **Supplementary Figure 1**).

Galeamopus

Fragmented and disarticulated pieces were rearticulated and placed at their assumed original positions. Missing and/or invisible parts were mirrored from the opposite side for *Galeamopus* and transformed using the *Lattice Deformer* in MAYA to align bilaterally exposed elements such as pre- and postzygapophyses to roughly estimate the hidden morphology and complete the partially exposed vertebrae.

The cervical vertebrae were initially retrodeformed using the retrodeform procedure in the IDAV LANDMARK editor (Lautenschlager, 2016) with a subset of the symmetrical

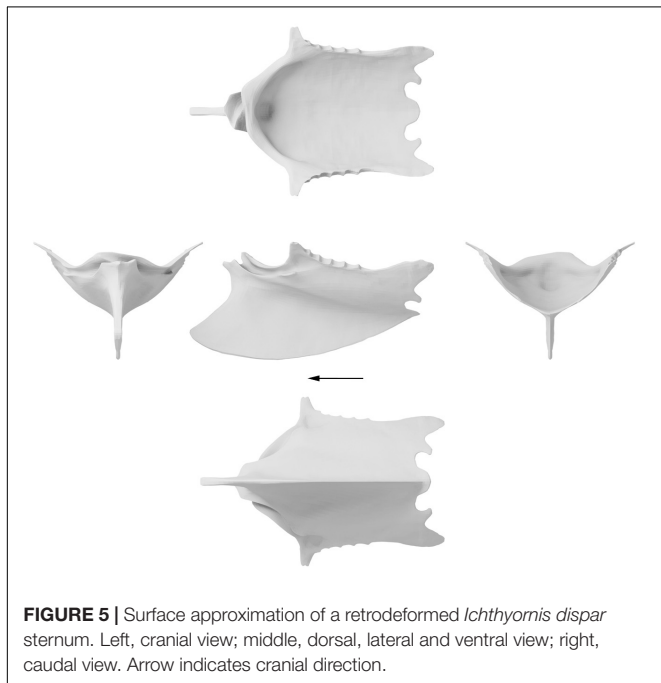
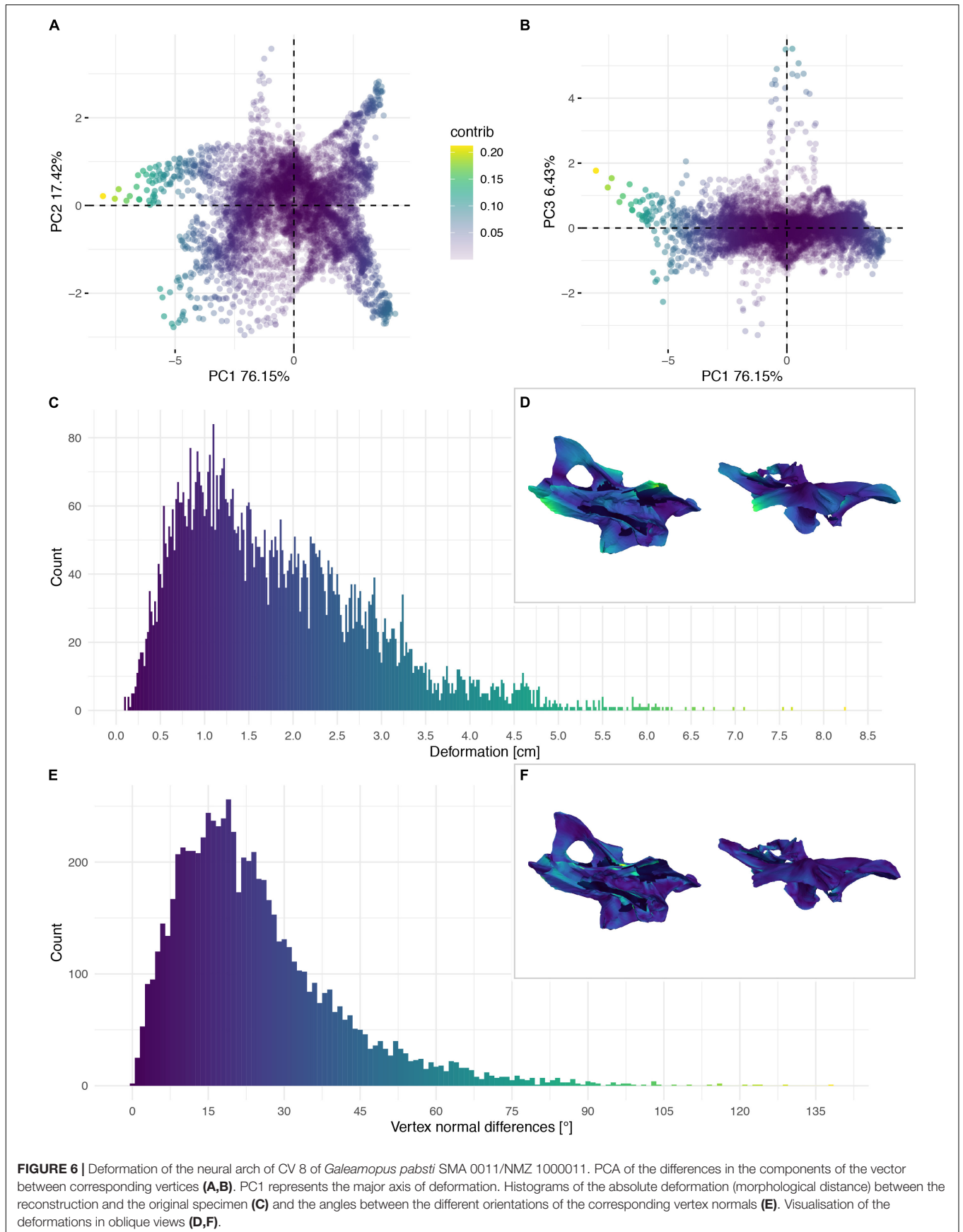
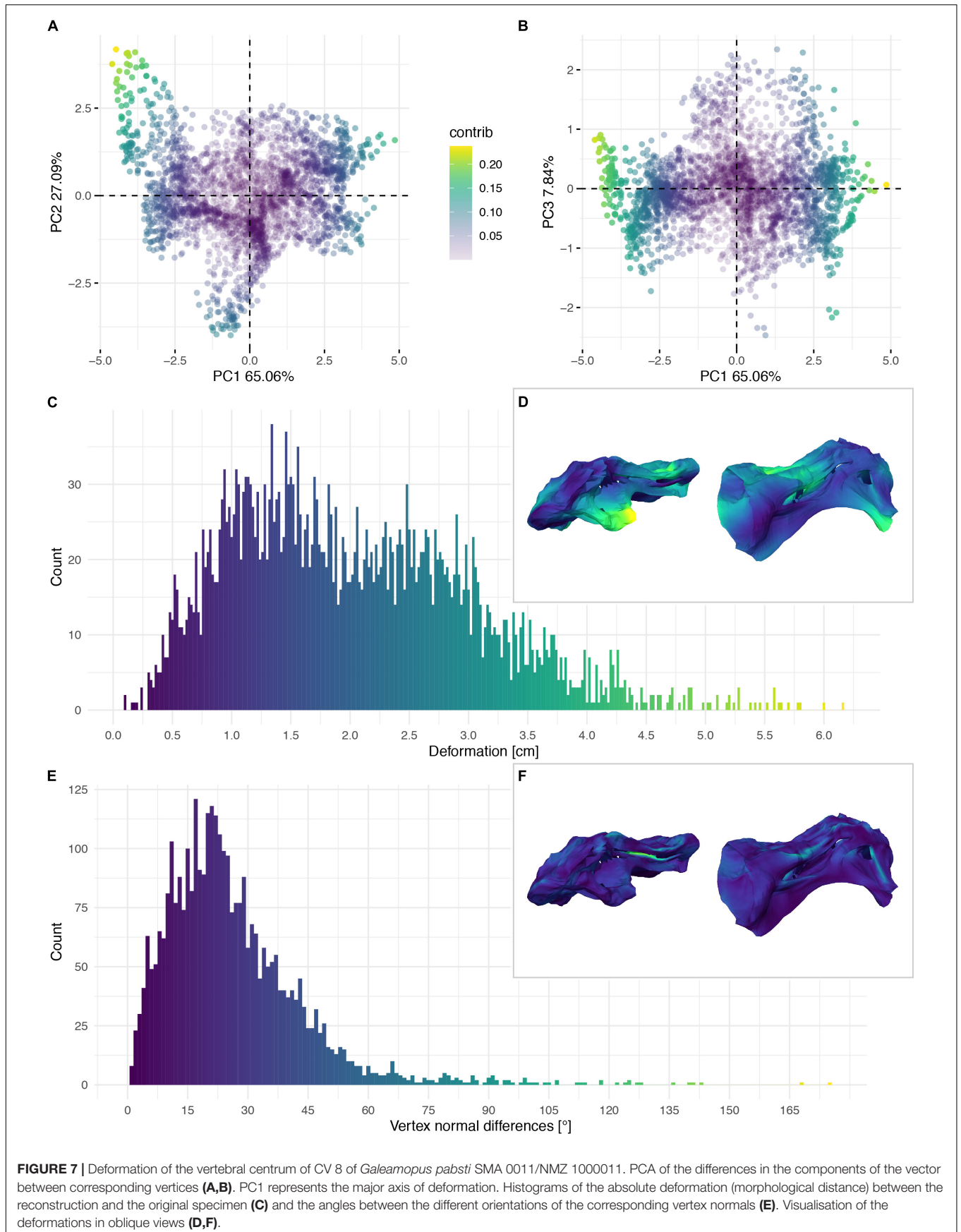
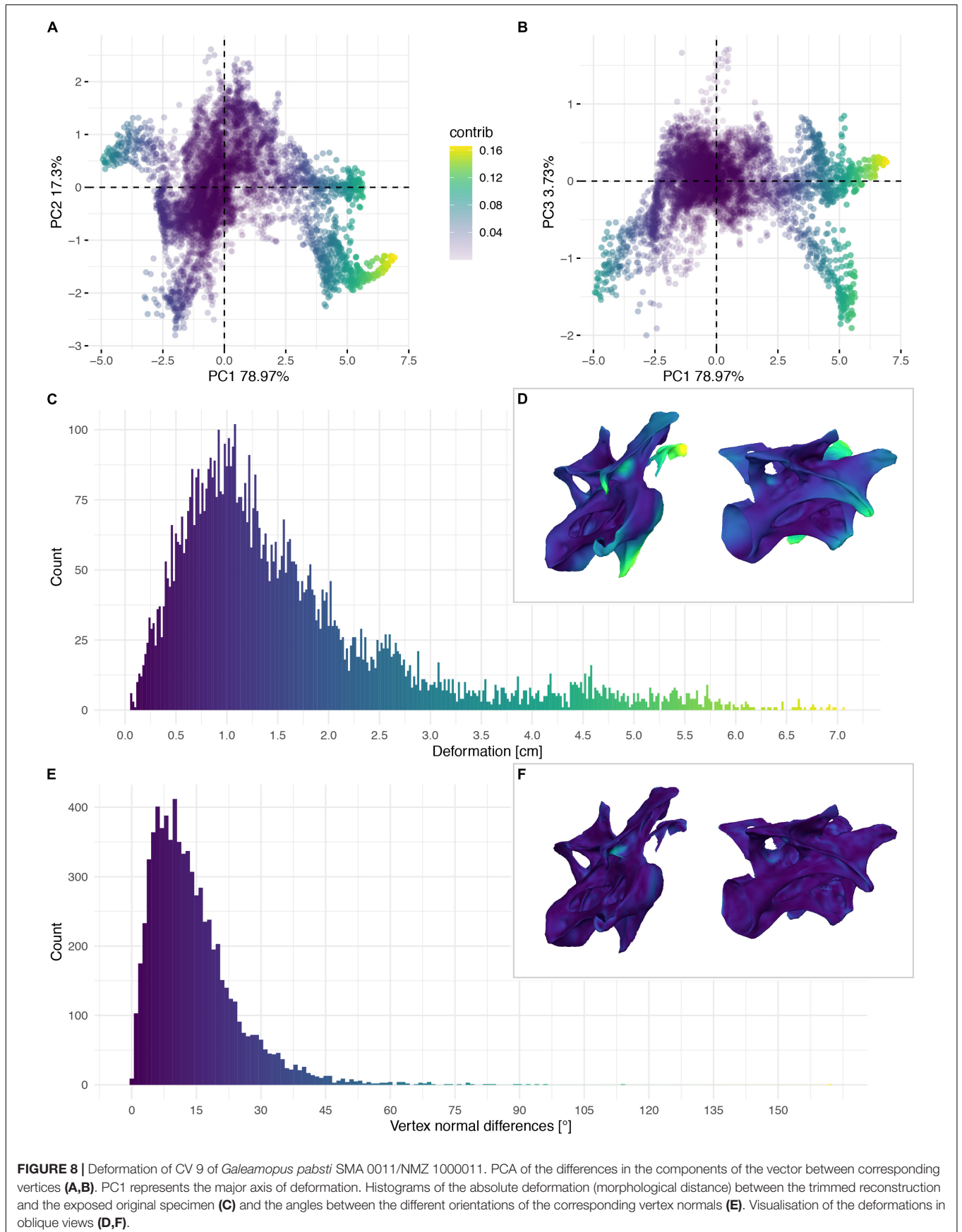
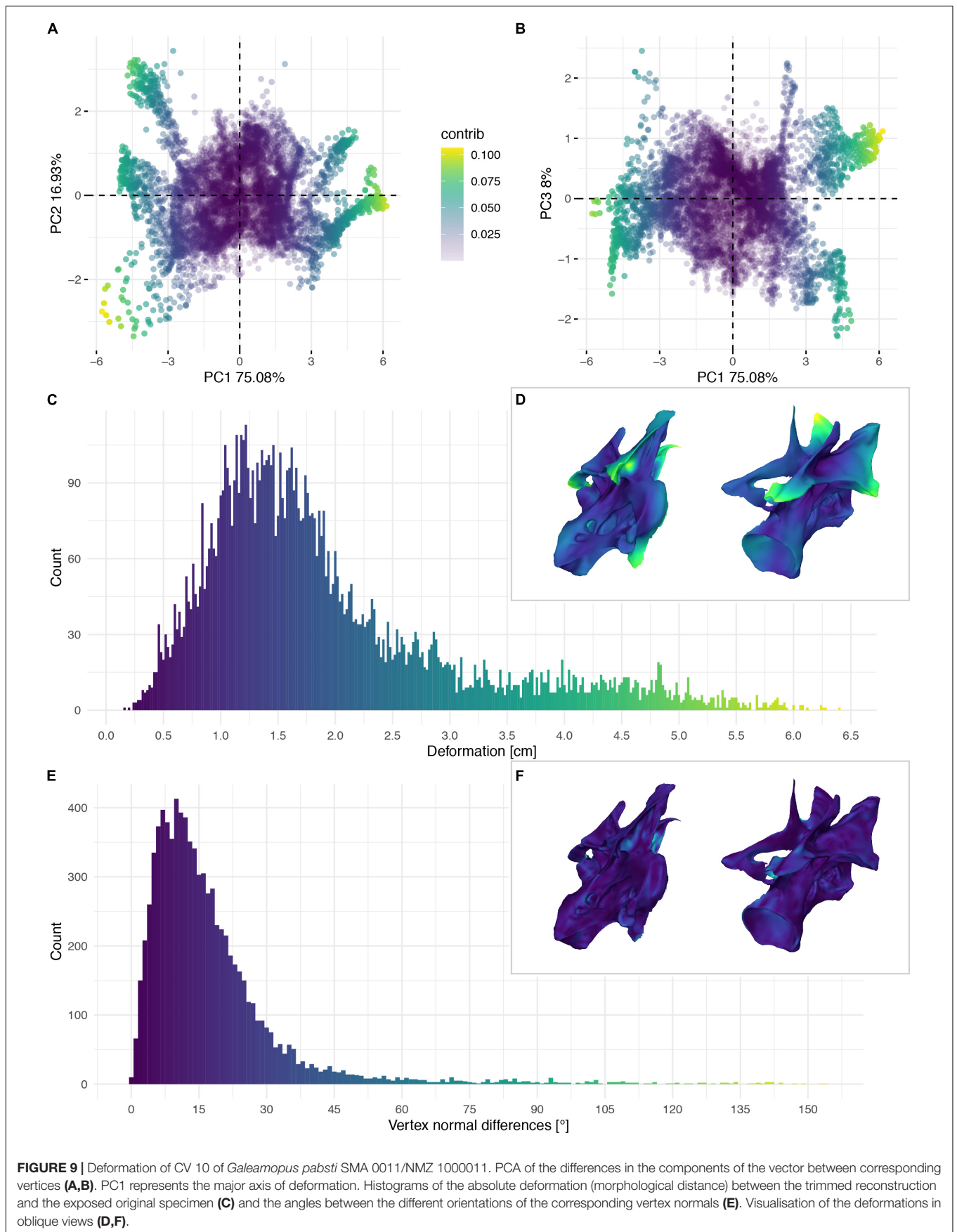


FIGURE 5 | Surface approximation of a retrodeformed *Ichthyornis dispar* sternum. Left, cranial view; middle, dorsal, lateral and ventral view; right, caudal view. Arrow indicates cranial direction.









landmarks across the sagittal plane (**Figure 3**) placed only on exposed bone. The retrodeformed vertebrae from LANDMARK were then fully symmetrised in MAYA through averaging the left and right sides (**Figure 3**). To accomplish this, the vertebrae were duplicated and mirrored and the vertices reordered to calculate the bilaterally average position of each vertex using a *blend shape* deformer with a weighting of 0.5. The vertebrae were subsequently adjusted to remove plastic deformation artefacts not covered through the LANDMARK retrodeformation and MAYA symmetrisation. To do so, the vertebrae were manually adjusted to reconstruct the assumed initially circular shape of the condyles and cotyles (Nyakatura et al., 2015) and the position and orientation of the pre- and postzygapophyses were slightly adjusted to bring them in line with the subsequent and/or preceding vertebrae. The diapophyses and laminae were adjusted to follow their general orientations in other less deformed flagellicaudatan sauropod specimens, such as *Kaatedocus siberi* SMA 0004/NMZ 1000004 (Tschopp and Mateus, 2013), *Diplodocus carnegii*

CM 84 (Hatcher, 1901) and *Apatosaurus louisae* CM 3018 (Gilmore, 1936).

Ichthyornis

The different specimens of *Ichthyornis* were compared, and individual well preserved regions, such as the crossed coracoid sulci in FHSM VP-18702 (**Supplementary Figure 2A**) or the craniolateral process and ventral lip of NHMUK PV A 905 (**Supplementary Figure 2B**), were detached from their original retotology meshes and combined into a new composite reconstruction. The well preserved coracoids KUVV 2281, ALMNH PV 1993.2.133, and YPM VP.001733 (Clarke, 2004; Benito et al., 2022) were used to assist in the shape reconstruction of the individual asymmetrical coracoid sulci while keeping their posterior margins symmetrical. The general shape and curvature of the lateral sternal plates were guided by sterna of comparable extant taxa, such as *Anas discors*, *Ardea alba*, *Burhinus oedichnemus*, and *Sterna hirundo* (Marsh, 1880; Clarke, 2004; Benito et al., 2022), while ensuring that the outline of

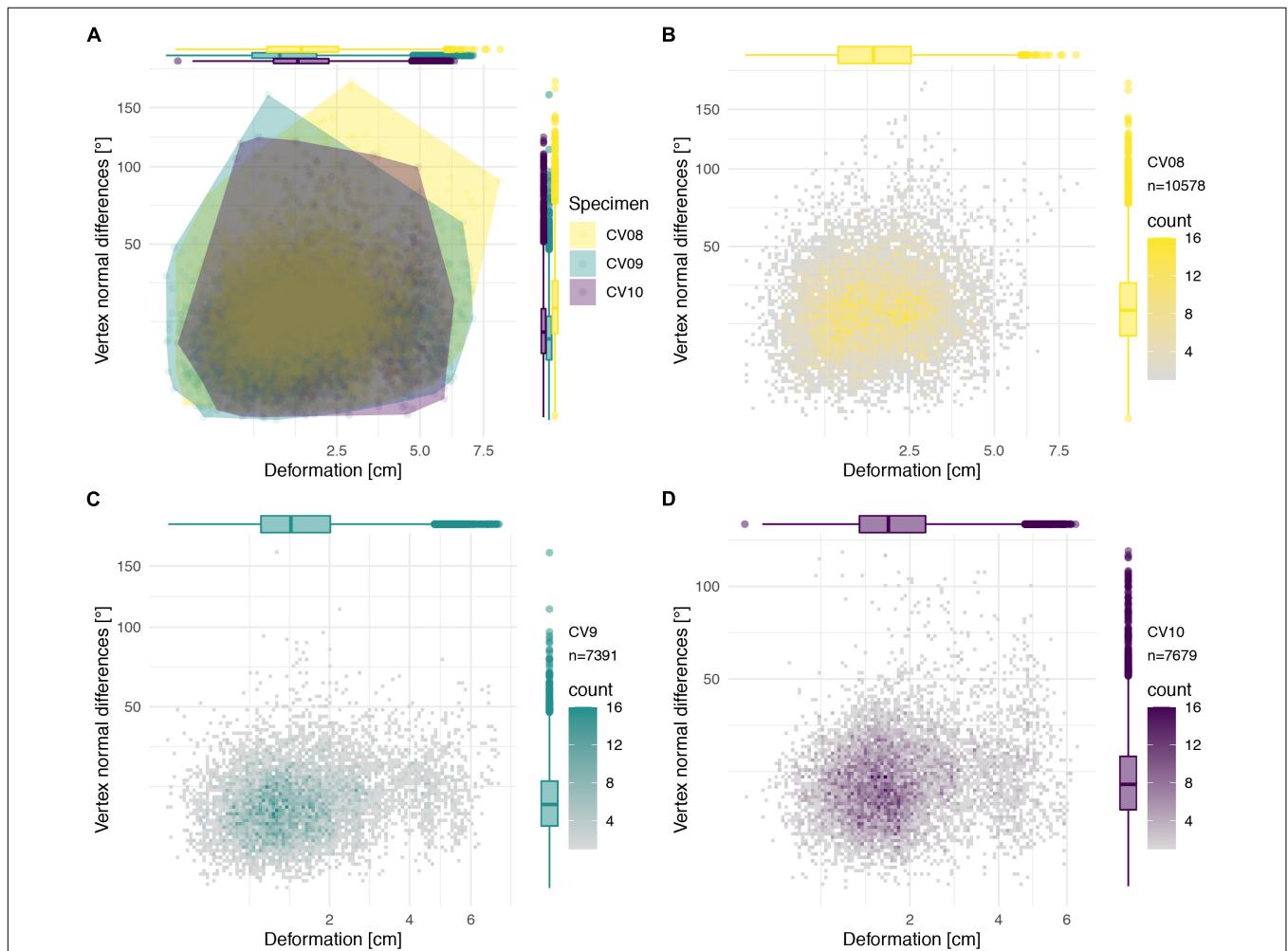


FIGURE 10 | Deformation comparison of the different vertebrae. Scatter plot of absolute global deformation (X-axis) and local deformation (Y-axis) of all vertebrae (**A**), combined arch and centrum of CV 8 (**B**), CV 9 (**C**), and CV 10 (**D**). Note the different number of landmarks “n” for each specimen.

the *Ichthyornis* sternum remained consistent with the preserved specimens (**Supplementary Figure 2C**).

Quantification of Deformation

Due to the targeted retopology of the individual specimens and the identical topology of the reconstructions, the specimens could be readily compared using geometric morphometric approaches. Each individual vertex (i.e., the global position of a mesh point) of the surface approximations acted as landmark for the shape comparison in the open-source software *R* (R Core Team, 2019). The reconstructions of the *Ichthyornis* sternum and the *Galeamopus* cervical vertebrae were trimmed for each comparison to match the preserved and/or exposed parts of the respective individual specimen by removing the missing vertices and faces, and their vertices were subsequently reordered in *MAYA* to receive corresponding point pairs. Trimmed surface approximations were loaded into *R* as Wavefront OBJ files and then processed through a generalised Procrustes analysis (GPA) using the *R* package *geomorph* (Adams et al., 2018) and subsequently analysed using the *R* package *FactoMineR* (Lê et al., 2008).

Global deformation was quantified as the distance between corresponding landmarks (i.e., vertices), similarly to previous studies (e.g., Di Vincenzo et al., 2017; Schlager et al., 2018; Cirilli et al., 2020; Bolet et al., 2021). However, shape variation between the original specimen and the reconstruction was visualised as heat maps using vertex colours in *MAYA* through a custom *MAYA* Embedded Language (MEL) script (**Supplementary Material**).

Due to the fact that the surface approximations consisted not only of vertices (representing landmarks) but were also connected through faces, additional information, such as the area or spatial orientation of individual faces and consequently of the vertices, could be obtained. For these calculations the surface approximations were triangulated so that three vertices described each individual face. A face normal represents a vector perpendicular to the plane described by its three vertices. Since each vertex could be part of multiple faces, the vertex normals were calculated as normalised summed vectors of the face normals of the surrounding faces multiplied by their in-face angle and face area. Local deformation was thus quantified as the change of orientation of the vertex normals in comparison between the retopologised deformed specimen and the trimmed reconstruction [i.e., the angle between the vectors representing the vertex normals, which is an addition to the repertoire of visualising local deformation (Piras et al., 2020)]. Additionally, individual face areas could be quantified and compared to visualise which areas were locally compressed during fossilisation, similar to the visualisations of deformation in Cirilli et al. (2020).

RESULTS

Reconstruction of the *Galeamopus* Cervical Vertebrae

Reconstructed CV 8 to 10 of *Galeamopus pabsti* SMA 0011/NMZ 1000011 are displayed in **Figure 4** and key metrics can be found in

Supplementary Table 3. The unfused and disarticulated centrum and neural arch of CV 8 were combined for the reconstruction. Cervical vertebrae 9 and 10 were both individually reconstructed.

Reconstruction of the *Ichthyornis* Sternum

The three-dimensional reconstruction of the *Ichthyornis* sternum consists of 11,444 vertices connected by 11,442 quadrilateral faces or 22,884 triangles (**Figure 5** and **Supplementary Table 4**). To enable comparison and evaluate the deformation of each of the individual specimens the reconstructed “prototype” was trimmed to only include vertices and faces present in each relevant specimen. Therefore, three additional adaptations of the reconstruction were created with differing numbers of vertices and faces, one for each of the specimens included in this study (**Supplementary Table 4**).

While some degree of skeletal asymmetry is present in all bilaterally symmetrical organisms, the magnitude is usually small and asymmetrical noise is usually filtered out in shape analyses (Hedrick et al., 2019). Large degrees of skeletal asymmetry are, by contrast, extremely rare in vertebrates due to developmental stability (Hedrick et al., 2019). Yet, if present, such as the crossed coracoid sulci in the sternum of *Ichthyornis* (**Figure 2** and **Supplementary Figure 2A**) or the skulls of echolocating whales (Coombs et al., 2020), such asymmetries represent a fundamental challenge to the general symmetrisation process of every retrodeformation protocol. Therefore, the coracoid sulci were separated from the rest of the sternum and thus excluded from the symmetrisation process. However, due to the fact that the asymmetrical coracoid sulci were bracketed by symmetrical elements (the sternal rostrum and keel cranially and ventrally, the coracoid pillar caudally and the craniolateral processes laterally), and were additionally preserved almost undistorted in FHSM VP-18702, they could be reincorporated into the symmetrised sternum reconstruction (**Figure 5**).

Quantification of Taphonomic Deformation

Taphonomic deformation of the individual specimens was evaluated as both global deformation (i.e., the morphological distance between the reconstruction and the deformed specimen), and local deformation (i.e., the difference in spatial orientation of the individual vertex normals, or the difference of the direction of the vector perpendicular to the planes described by surrounding vertices). All specimens showed a wide range of global and local deformation; however, the specimens showed individual differences related to their specific deformation histories. Principal component analysis (PCA) of global deformation revealed the major deformation axes, with PC1 corresponding to the main axis along which the specimens were compressed and/or sheared. Areas within a specimen with high degrees of local deformation could be attributed to folding or shearing of an area in relation to another resulting in large differences in angles relative to the idealised reconstruction.

Galeamopus

Individual global and local deformation of each vertebra was quantified through morphological comparisons of the retopologised exposed bone with the trimmed down reconstruction of each respective vertebra (Figures 6–9). The disarticulated centrum and neural arch of CV8 were compared individually (Figures 6, 7) but combined for the comparison of all reconstructed vertebrae (Figure 10). There appears to be no clear correlation between the degree of global and local deformation in any of the three reconstructed vertebrae (Figure 10). PC1 explains 65% of deformation for the centrum of CV8 and more than 75% of CV9 and CV10 as well as the arch of CV8 attributable to this axis, with the other PC axes representing only relatively minor contributions to overall deformation.

Ichthyornis

The deformation of the *Ichthyornis* sterna could be quantified in each individual specimen by comparison to the trimmed “prototype” reconstructions matching their individual topology and vertex count. This, however, complicated direct comparisons among all specimens, as some landmarks were present in some specimens but not in others. Nonetheless, the individual specimens could be compared to examine patterns in their deformation (Figures 11–14), as the relationship between global and local deformations was investigated irrespective of their exact landmark configuration. Whereas the sterna of NHMUK PV A905 and KUVV 119673 were primarily unilaterally flattened, FHSM VP-18702 was mediolaterally compressed and folded, and thus showed more overall deformation than the other two specimens (Figure 14A). Overall, FHSM VP-18702 showed the greatest deformation disparity of the three specimens, occupying the greatest area of both local and global deformation axes, which is likely related to its greater degree of completeness with respect to the other specimens. If more disparate points are represented in a specimen (e.g., FHSM VP-18702 uniquely preserves both lateral plates of the sternum), then depending on the direction of deformation they experienced, this increased surface area might naturally exhibit a higher degree of global deformation than a more fragmentary element, as peripheral landmarks might be displaced more than centrally positioned ones, especially in mediolateral compression as FHSM VP-18702 experienced (Figure 12).

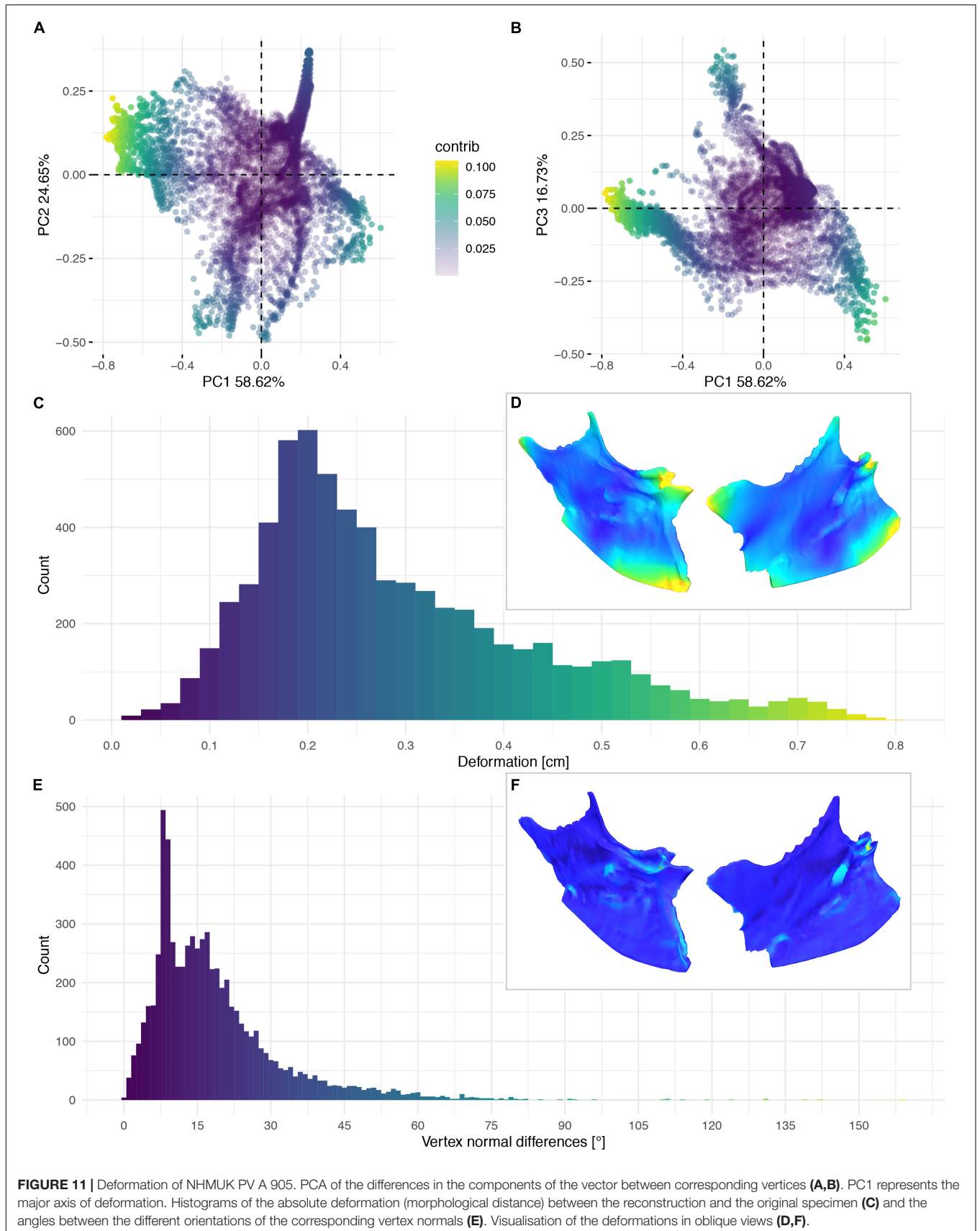
The cluster of local deformation of around 10° with varying degrees of morphological distance between the reconstruction and the original, deformed, NHMUK PV A905 (Figure 14B) suggests that a localised area experienced a consistent change of orientation with increasing spatial distance during the deformation. Thus, this pattern probably results from a single breakage and folding of that localised area. In contrast, the cluster of around 0.9 cm of deformation with various angles in FHSM VP-18702 (Figure 14D) captures complex folding and bending with little variation in offset in a subarea of the posterior left lateral plate in this specimen. In KUVV 119673 no clear pattern of deformation could be observed, with both global and local deformation being widely distributed with no obvious correlations among them (Figure 14C).

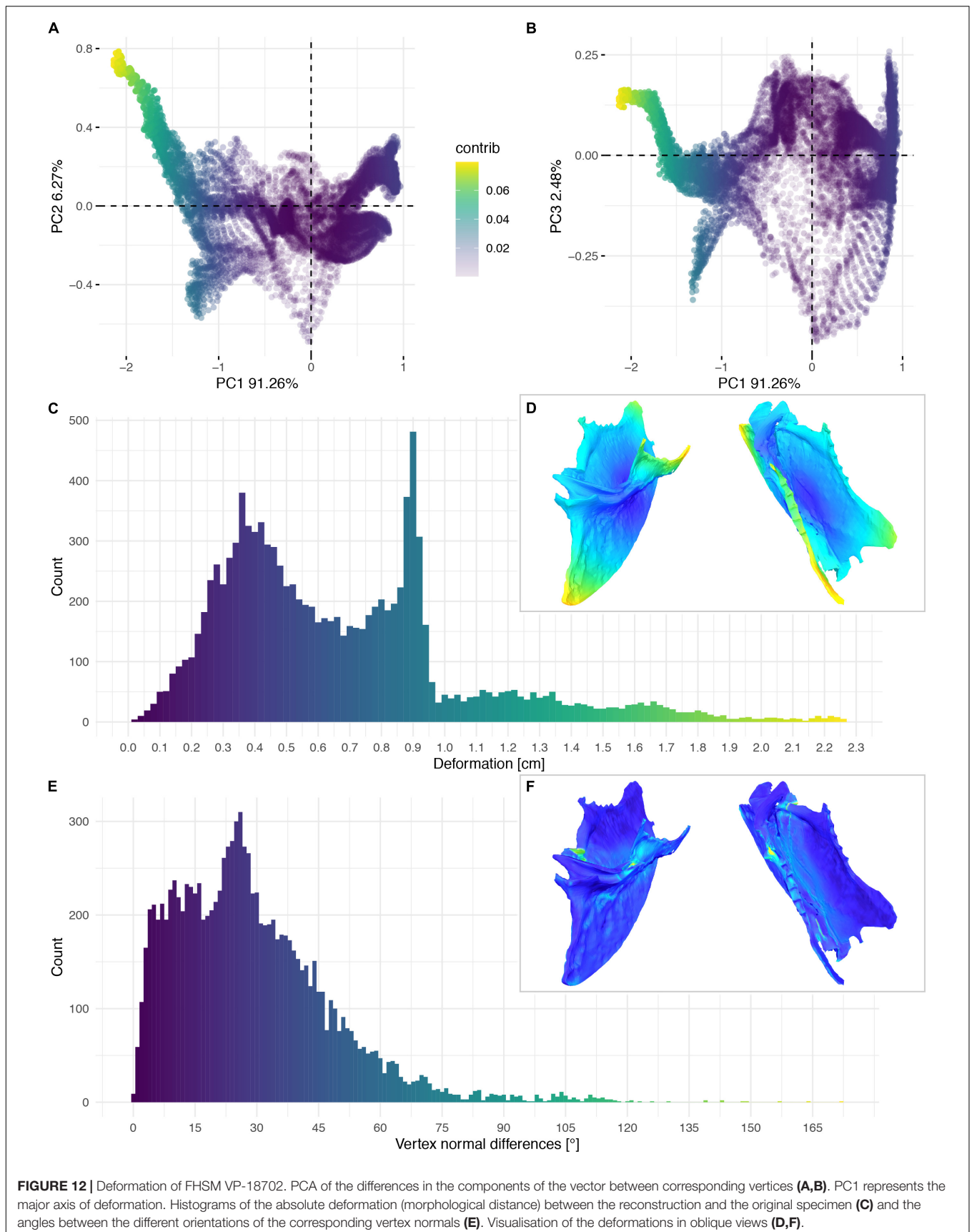
DISCUSSION

We present our hard tissue reconstructions as hypothetical and idealised surface approximations. There is always an unavoidable degree of uncertainty regarding three-dimensional reconstructions of taphonomically deformed skeletal elements. The accuracy of a reconstruction process is inevitably difficult to measure, unless an entirely undistorted specimen exists as the basis for direct comparisons (see Tallman et al., 2014; Schlager et al., 2018; Cirilli et al., 2020). However, even automated retrodeformation approaches can lead to multiple different results depending on the degree of initial deformation (Tschopp et al., 2013; Tallman et al., 2014; Vidal and Díez Díaz, 2017), and may not produce an adequate reconstruction of a deformed specimen’s true *in vivo* morphology (Supplementary Figure 1; Tschopp et al., 2013; Hedrick et al., 2019). Such situations necessitate the inclusion of sensitivity analyses to address uncertainties in potential downstream analyses (Bishop et al., 2021).

The retrodeformation methodology presented herein has some caveats based on two key assumptions underlying the reconstruction process:

- (1) The method generally assumes bilateral symmetry in the initial object, although it can in theory be applied to generally asymmetrical objects (e.g., long bones), if at least two of them are preserved; however, results for such objects may be less reliable than for symmetrical objects (see Hedrick et al., 2019; Pintore et al., 2022). Small individual shape variation and fluctuating asymmetry cannot be taken into account directly. In complex sauropod vertebrae, certain asymmetrical and irregular accessory laminae are thus impossible to fully represent with this method, as both sides get symmetrised. Asymmetrical portions of generally symmetrical objects, such as the crossed coracoid sulci of *Ichthyornis*, can, however, be specifically excluded from the generalised symmetrisation process and later reincorporated into the reconstruction, since they are bracketed by symmetrical elements. This process therefore allows reconstructing virtually any mostly bilaterally symmetrical bone, while allowing some localised asymmetry to be maintained.
- (2) This methodology produces a simplification and idealisation of the general shape of any given bone. This enables the reconstruction of the gross morphology, but surface details and textures cannot directly be preserved, and the reconstruction thus needs to be interpreted as an idealised “prototype” of the object. This could, however, be mitigated in combination with morphing tools applied on top of the retopologised object, allowing the initial shape to be morphed into the new “prototype” by using the individual vertices as landmarks, thus potentially retaining detailed surface information with minimal artificial distortion. However, such high-fidelity reconstructions are often not desirable as they increase computation time for





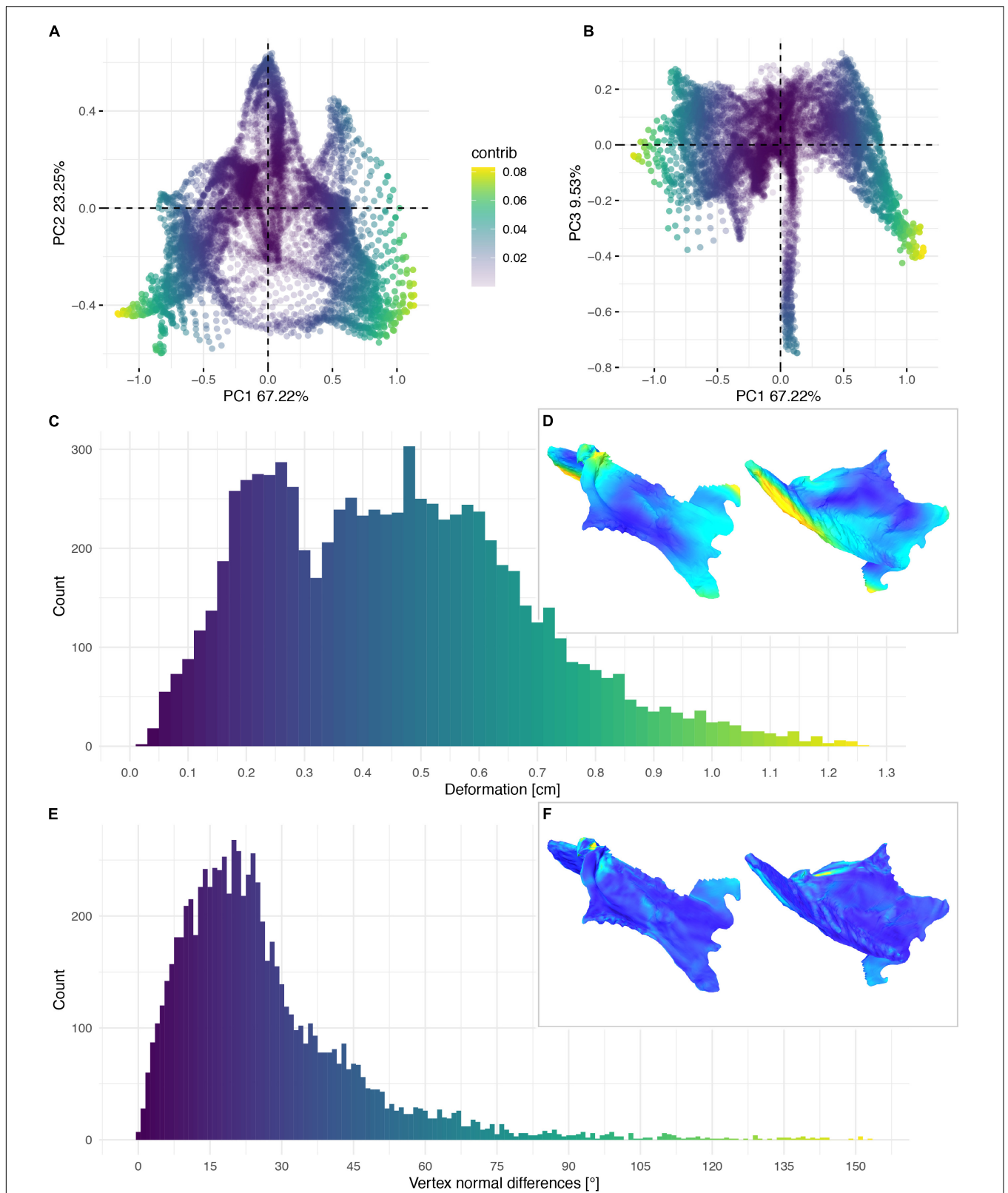
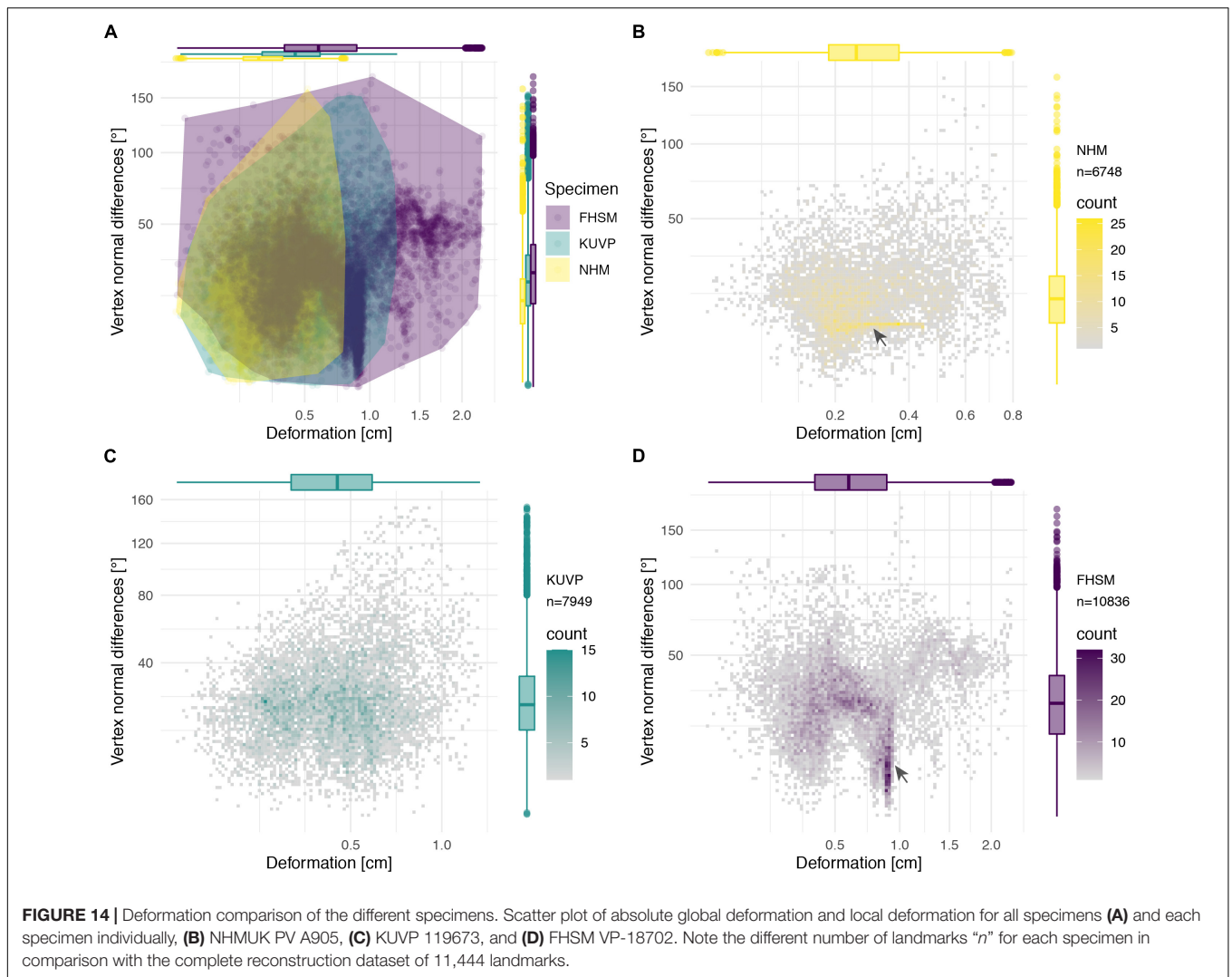


FIGURE 13 | Deformation of KUVP 119673. PCA of the global differences in the components of the vector between corresponding vertices (**A,B**). PC1 represents the major axis of deformation. Histograms of the absolute deformation (morphological distance) between the reconstruction and the original specimen (**C**) and the angles between the different orientations of the corresponding vertex normals (**E**). Visualisation of the deformations in oblique views (**D,F**).



downstream analyses, such as biomechanical analyses (e.g., FEA) and surface approximations are often sufficient

(Rahman and Lautenschlager, 2017; Morales-García et al., 2019; Lautenschlager et al., 2020). Furthermore, detailed surface information might result from local deformation rather than original morphology, so the morphing of the original surface of the fossil into the reconstructed shape may introduce more taphonomic artefacts than real biological information. It is therefore not advised to simply morph the original object into the new “prototype” shape. Additionally, imprecision in the vertex placement can inadvertently distort localised areas if the original object is morphed, while the “prototype” itself is not affected by any initial imprecision. The idealisation might instead represent a more accurate but less precise reconstruction.

Our approach is not limited to reconstructing deformed skeletal remains, but also has potential in investigating, quantifying and comparing shape variation in minute detail. Variation among serial elements, such as vertebrae, haemal arches or ribs, could be investigated (e.g., see Marek et al., 2021; Müller

et al., 2021) to test whether, how many, and in which position serial elements might be missing, and then to automatically interpolate missing mediotypes to fill in the gaps.

The reconstruction methodology presented here focuses solely on hard tissue remains (i.e., fossilised bones) and is partially dependent on the quality of the remains. Aspects of this approach are therefore unlikely to be directly applicable to soft tissue remains because of their often-pliable nature, which would be expected to prevent the reliable estimation of their original morphology. However, the potential applicability of this methodology to well preserved soft tissue remains will require further investigation.

CONCLUSION

Our proposed retopology and reconstruction workflow facilitates the integration of partial specimens into a composite reconstruction and enables quantification and visualisation of their taphonomic deformation. The lower resolution of the surface approximation, in comparison with high fidelity scan

data, allows for more control in the reconstruction process, and facilitates downstream analyses with shorter computation times.

The inclusion of faces in shape analyses allows the quantification of vertex and face orientation, adding another possibility to capture and analyse local shape disparity. Mean shapes of conventional landmark datasets can be triangulated and the triangulation matrix applied to the other samples to enable these additional comparisons.

The method presented here represents a significant advance in our ability to overcome the challenges imposed by taphonomic deformation of fossils, and provides new, robust approaches for quantifying the extent and nature of taphonomic deformation. We anticipate that this approach will prove useful for a wide range of palaeobiological applications.

DATA AVAILABILITY STATEMENT

The data generated in this study are included directly in the article and **Supplementary Material**. The digital 3D models of the specimens presented herein and their reconstructions are available on MorphoSource under the project “Deformation Quantification” (ID: 000411920; <https://www.morphosource.org/projects/000411920>). The MEL (MAYA Embedded Language) script for the visualization of CSV data as heat maps through vertex colors is provided in the Supplementary Material. Several **Supplementary Videos (S1–S15)** illustrating the taphonomic global and local deformation of each specimen are also provided (**Supplementary Datas S1–S7**). A complete list of the specimens and digitized elements used in this study is provided in **Supplementary Table S1**, including links to the online repository MorphoSource for each individual 3D model.

AUTHOR CONTRIBUTIONS

OD, ET, NH, and DF conceived and designed this study. OD, JB, ET, HM, and DF collected the bone surface data. SL assisted in the retrodeformation process. OD analysed and interpreted

the data, prepared the figures, and wrote the manuscript. All authors contributed to editing and revisions of the manuscript and approved the final version.

FUNDING

DF acknowledges support from UKRI Future Leaders Fellowship MR/S032177/1. ET was supported by the doctoral fellowship SFRH/BD/66209/2009 awarded by the Fundação para a Ciência e a Tecnologia of the Ministério de Educação e Ciência (FCT-MEC), Portugal. JB acknowledges support from the Palaeontographical Society Richard Owen Research fund and from the University of Bath University Research Studentship Award.

ACKNOWLEDGMENTS

We are very grateful to Karin Seiler and David Schürch (ZHdK) for their valuable input during the initial conception of this project and thank the members of Knowledge Visualization at the Zurich University of the Arts (ZHdK) for assistance during the initial stages of project development. We thank Hans-Jakob “Kirby” Siber, Thomas Bolliger, Ben Pabst, Rabea Lillich, and Esther Wolfensberger (SMA), and Christian Klug and Dennis Hansen (PIM UZH) for access to SMA 0011/NMZ 1000011. We thank Matt Colbert and Keturah Smithson for scans of *Ichthyornis*. We further thank Jonas Lauströer (HAW Hamburg) for fruitful discussions, and MP and MR for their constructive reviewer feedback.

SUPPLEMENTARY MATERIAL

The Supplementary Material for this article can be found online at: <https://www.frontiersin.org/articles/10.3389/fevo.2022.828006/full#supplementary-material>

REFERENCES

- Adams, D. C., Collyer, M. L., and Kaliontzopoulou, A. (2018). *Geomorph: Software for Geometric Morphometric Analyses. R Package Version 3.0.6*. Available online at: <https://cran.r-project.org/package=geomorph> (accessed January 31, 2021).
- Ahlberg, P. E., and Milner, A. R. (1994). The origin and early diversification of tetrapods. *Nature* 368, 507–514. doi: 10.1038/368507a0
- Alroy, J. (2010). Fair sampling of taxonomic richness and unbiased estimation of origination and extinction rates. *Paleontol. Soc. Pap.* 16, 55–80. doi: 10.1017/S1089332600001819
- Angielczyk, K. D., and Sheets, H. D. (2007). Investigation of simulated tectonic deformation in fossils using geometric morphometrics. *Paleobiology* 33, 125–148. doi: 10.1666/06007.1
- Arbour, V. M., and Currie, P. J. (2012). Analyzing taphonomic deformation of ankylosaur skulls using retrodeformation and finite element analysis. *PLoS One* 7:e39323. doi: 10.1371/journal.pone.0039323
- Bardua, C., Felice, R. N., Watanabe, A., Fabre, A.-C., and Goswami, A. (2019). A practical guide to sliding and surface semilandmarks in morphometric analyses. *Integr. Org. Biol.* 1:obz016. doi: 10.1093/iob/obz016
- Baumel, J. J., and Witmer, L. M. (1993). “Osteologia,” in *Handbook of Avian Anatomy: Nomina Anatomica Avium*, ed. J. J. Baumel (Cambridge, MA: Nuttall Ornithological Club), 45–132.
- Belvedere, M., Bennett, M. R., Marty, D., Budka, M., Reynolds, S. C., and Bakirov, R. (2018). Stat-tracks and mediotypes: powerful tools for modern ichnology based on 3D models. *PeerJ* 6:e4247. doi: 10.7717/peerj.4247
- Benito, J., Chen, A., Bhullar, B.-A., Burnham, D., Wilson, L. E., and Field, D. J. (2022). 40 new specimens of *Ichthyornis* provide unprecedented insight into the postcranial morphology of crownward stem group birds. *bioRxiv* [preprint] doi: 10.1101/2022.01.11.475364
- Benton, M. J., and Harper, D. A. T. (eds). (2009). “Taphonomy and the quality of the fossil record,” in *Introduction to Paleobiology and the Fossil Record*, 1st Edn (Hoboken, NJ: Wiley-Blackwell), 57–78.
- Bishop, P. J., Cuff, A. R., and Hutchinson, J. R. (2021). How to build a dinosaur: musculoskeletal modeling and simulation of locomotor biomechanics in extinct animals. *Paleobiology* 47, 1–38. doi: 10.1017/pab.2020.46
- Bolet, A., Stanley, E. L., Daza, J. D., Arias, J. S., Čerňanský, A., Vidal-García, M., et al. (2021). Unusual morphology in the mid-Cretaceous lizard *Oculudentavis*. *Curr. Biol.* 31, 3303–3314.e3. doi: 10.1016/j.cub.2021.05.040

- Bommes, D., Lévy, B., Pietroni, N., Puppo, E., Silva, C., Tarini, M., et al. (2013). Quad-mesh generation and processing: a survey. *Comput. Graph. Forum* 32, 51–76. doi: 10.1111/cgf.12014
- Bommes, D., Zimmer, H., and Kobbelt, L. (2009). Mixed-integer quadrangulation. *ACM Trans. Graph.* 28, 1–10. doi: 10.1145/1531326.1531383
- Bonaparte, J. F. (1999). Evolución de las vértebras presacras en Sauropodomorpha. *Ameghiniana* 36, 115–187.
- Brocklehurst, N., Upchurch, P., Mannion, P. D., and O'Connor, J. (2012). The completeness of the fossil record of mesozoic birds: implications for early avian evolution. *PLoS One* 7:e39056. doi: 10.1371/journal.pone.0039056
- Cashmore, D. D., Mannion, P. D., Upchurch, P., and Butler, R. J. (2020). Ten more years of discovery: revisiting the quality of the Sauropodomorph dinosaur fossil record. *Palaeontology* 63, 951–978. doi: 10.1111/pala.12496
- Cerda, I. A., Salgado, L., and Powell, J. E. (2012). Extreme postcranial pneumaticity in sauropod dinosaurs from South America. *Paläontol. Z.* 86, 441–449. doi: 10.1007/s12542-012-0140-6
- Cirilli, O., Melchionna, M., Serio, C., Bernor, R. L., Bukhsianidze, M., Lordkipanidze, D., et al. (2020). Target Deformation of the *Equus stenonis* holotype skull: a virtual reconstruction. *Front. Earth Sci.* 8:247. doi: 10.3389/feart.2020.00247
- Clarke, J. A. (2004). Morphology, phylogenetic taxonomy, and systematics of *Ichthyornis* and *Apatornis* (Avalae: Ornithurae). *Bull. Am. Mus. Nat. Hist.* 286, 1–179. doi: 10.1206/0003-0090(2004)286<0001:mptaso>2.0.co;2
- Coombs, E. J., Clavel, J., Park, T., Churchill, M., and Goswami, A. (2020). Wonky whales: the evolution of cranial asymmetry in cetaceans. *BMC Biol.* 18:86. doi: 10.1186/s12915-020-00805-4
- Cuff, A. R., and Rayfield, E. J. (2015). Retrodeformation and muscular reconstruction of ornithomimosaurian dinosaur crania. *PeerJ* 3:e1093. doi: 10.7717/peerj.1093
- Cunningham, J. A., Rahman, I. A., Lautenschlager, S., Rayfield, E. J., and Donoghue, P. C. J. (2014). A virtual world of paleontology. *Trends Ecol. Evol.* 29, 347–357. doi: 10.1016/j.tree.2014.04.004
- Currey, J. D., and Alexander, R. M. (1985). The thickness of the walls of tubular bones. *J. Zool.* 206, 453–468. doi: 10.1111/j.1469-7998.1985.tb03551.x
- Daeschler, E. B., Shubin, N. H., and Jenkins, F. A. (2006). A Devonian tetrapod-like fish and the evolution of the tetrapod body plan. *Nature* 440, 757–763. doi: 10.1038/nature04639
- Davies, T. G., Rahman, I. A., Lautenschlager, S., Cunningham, J. A., Asher, R. J., Barrett, P. M., et al. (2017). Open data and digital morphology. *Proc. R. Soc. B Biol. Sci.* 284:20170194. doi: 10.1098/rspb.2017.0194
- Demuth, O. E., Wiseman, A. L. A., van Beesel, J., Mallison, H., and Hutchinson, J. R. (2022). Three-dimensional polygonal muscle modelling and line of action estimation in living and extinct taxa. *Sci. Rep.* 12:3358. doi: 10.1038/s41598-022-07074-x
- Di Vincenzo, F., Profico, A., Bernardini, F., Cerroni, V., Dreossi, D., Schlager, S., et al. (2017). Digital reconstruction of the *Ceprano calvarium* (Italy), and implications for its interpretation. *Sci. Rep.* 7:13974. doi: 10.1038/s41598-017-14437-2
- Diez Diaz, V., Mallison, H., Asbach, P., Schwarz, D., and Blanco, A. (2021). Comparing surface digitization techniques in palaeontology using visual perceptual metrics and distance computations between 3D meshes. *Palaeontology* 64, 179–202. doi: 10.1111/pala.12518
- Field, D. J., Hanson, M., Burnham, D., Wilson, L. E., Super, K., Ehret, D., et al. (2018). Complete *Ichthyornis* skull illuminates mosaic assembly of the avian head. *Nature* 557, 96–100. doi: 10.1038/s41586-018-0053-y
- Foth, C., and Rauhut, O. W. M. (2013). The good, the bad, and the ugly: the influence of skull reconstructions and intraspecific variability in studies of cranial morphometrics in theropods and basal saurischians. *PLoS One* 8:e72007. doi: 10.1371/journal.pone.0072007
- Fountaine, T. M. R., Benton, M. J., Dyke, G. J., and Nudds, R. L. (2005). The quality of the fossil record of Mesozoic birds. *Proc. R. Soc. B Biol. Sci.* 272, 289–294. doi: 10.1098/rspb.2004.2923
- Gauthier, J. A., Kluge, A. G., and Rowe, T. (1988). Amniote phylogeny and the importance of fossils. *Cladistics* 4, 105–209. doi: 10.1111/j.1096-0031.1988.tb00514.x
- Ghosh, D., Amenta, N., and Kazhdan, M. (2010). Closed-form blending of local symmetries. *Comput. Graph. Forum* 29, 1681–1688. doi: 10.1111/j.1467-8659.2010.01777.x
- Gilmore, C. W. (1936). Osteology of *Apatosaurus* with special reference to specimens in the Carnegie Museum. *Mem. Carnegie Mus.* 11, 175–300.
- Golovinskiy, A., Podolak, J., and Funkhouser, T. (2009). “Symmetry-aware mesh processing,” in *Mathematics of Surfaces XIII. Mathematics of Surfaces 2009. Lecture Notes in Computer Science*, Vol. 5654, eds E. R. Hancock, R. R. Martin, and M. A. Sabin (Berlin: Springer), 170–188. doi: 10.1007/978-3-642-03596-8_10
- Gunz, P., Mitteroecker, P., and Bookstein, F. (2005). “Semilandmarks in three dimensions,” in *Modern Morphometrics in Physical Anthropology*, ed. D. E. Slice (New York, NY: Plenum Publishers), 73–98. doi: 10.1007/0-387-27614-9
- Gunz, P., Mitteroecker, P., Neubauer, S., Weber, G. W., and Bookstein, F. L. (2009). Principles for the virtual reconstruction of hominin crania. *J. Hum. Evol.* 57, 48–62. doi: 10.1016/j.jhevol.2009.04.004
- Hatcher, J. B. (1901). *Diplodocus* (Marsh): its osteology, taxonomy, and probable habits, with restoration of the skeleton. *Mem. Carnegie Mus.* 1, 1–63. doi: 10.5005/jp/books/11085_1
- Hedrick, B. P., Schachner, E. R., Rivera, G., Dodson, P., and Pierce, S. E. (2019). The effects of skeletal asymmetry on interpreting biologic variation and taphonomy in the fossil record. *Paleobiology* 45, 154–166. doi: 10.1017/pab.2018.42
- Hsiang, A. Y., Field, D. J., Webster, T. H., Behlke, A. D. B., Davis, M. B., Racicot, R. A., et al. (2015). The origin of snakes: revealing the ecology, behavior, and evolutionary history of early snakes using genomics, phenomics, and the fossil record. *BMC Evol. Biol.* 15:87. doi: 10.1186/s12862-015-0358-5
- Kammerer, C. F., Deutsch, M., Lungmus, J. K., and Angielczyk, K. D. (2020). Effects of taphonomic deformation on geometric morphometric analysis of fossils: a study using the dicynodont *Diictodon feliceps* (Therapsida, Anomodontia). *PeerJ* 8:e9925. doi: 10.7717/peerj.9925
- Kazhdan, M., Amenta, N., Gu, S., Wile, D. F., and Hamann, B. (2009). “Symmetry restoration by stretching,” in *Proceedings of the 21st Annual Canadian Conference on Computational Geometry, CCCG 2009*, Vancouver, BC, 37–40.
- Lambertz, M., Bertozzo, F., and Sander, P. M. (2018). Bone histological correlates for air sacs and their implications for understanding the origin of the dinosaurian respiratory system. *Biol. Lett.* 14:20170514. doi: 10.1098/rsbl.2017.0514
- Lautenschlager, S. (2016). Reconstructing the past: methods and techniques for the digital restoration of fossils. *R. Soc. Open Sci.* 3:160342. doi: 10.1098/rsos.160342
- Lautenschlager, S., and Rücklin, M. (2014). Beyond the print—virtual paleontology in science publishing, outreach, and education. *J. Paleontol.* 88, 727–734. doi: 10.1666/13-085
- Lautenschlager, S., Figueirido, B., Cashmore, D. D., Bendel, E.-M., and Stubbs, T. L. (2020). Morphological convergence obscures functional diversity in sabretoothed carnivores. *Proc. R. Soc. B Biol. Sci.* 287:20201818. doi: 10.1098/rspb.2020.1818
- Lê, S., Josse, J., and Husson, F. (2008). FactoMineR: an R package for multivariate analysis. *J. Stat. Softw.* 25, 253–258.
- Livezey, B. C., and Zusi, R. L. (2006). Higher-order phylogeny of modern birds (Theropoda, Aves: Neornithes) based on comparative anatomy: I. methods and characters. *Bull. Carnegie Mus. Nat. Hist.* 37, 1–544. doi: 10.1111/j.1096-3642.2006.00293.x
- Mallison, H., and Wings, O. (2014). Photogrammetry in paleontology – a practical guide. *J. Paleontol. Tech.* 12, 1–31. doi: 10.1130/micro21-p1
- Mannion, P. D., and Upchurch, P. (2010). Completeness metrics and the quality of the sauropodomorph fossil record through geological and historical time. *Paleobiology* 36, 283–302. doi: 10.1666/09008.1
- Marek, R. D., Falkingham, P. L., Benson, R. B. J., Gardiner, J. D., Maddox, T. W., and Bates, K. T. (2021). Evolutionary versatility of the avian neck. *Proc. R. Soc. B Biol. Sci.* 288:20203150. doi: 10.1098/rspb.2020.3150
- Marsh, O. C. (1880). *Odontornithes: A Monograph on the Extinct Toothed Birds of North America*. Washington, DC: Government Printing Office. doi: 10.5962/bhl.title.61298
- Mitra, N. J., Guibas, L. J., and Pauly, M. (2006). Partial and approximate symmetry detection for 3D geometry. *ACM Trans. Graph.* 25, 560–568. doi: 10.1145/1141924
- Mitra, N. J., Guibas, L. J., and Pauly, M. (2007). Symmetrization. *ACM Trans. Graph.* 26:63. doi: 10.1145/1239451.1239514

- Molnar, J., Pierce, S., Clack, J., and Hutchinson, J. (2012). Idealized landmark-based geometric reconstructions of poorly preserved fossil material: a case study of an early tetrapod vertebra. *Palaeontol. Electron.* 15, 1–18. doi: 10.26879/274
- Morales-García, N. M., Burgess, T. D., Hill, J. J., Gill, P. G., and Rayfield, E. J. (2019). The use of extruded finite-element models as a novel alternative to tomography-based models: a case study using early mammal jaws. *J. R. Soc. Interface* 16:20190674. doi: 10.1098/rsif.2019.0674
- Motani, R. (1997). New technique for retrodeforming tectonically deformed fossils, with an example for ichthyosaurian specimens. *Lethaia* 30, 221–228. doi: 10.1111/j.1502-3931.1997.tb00464.x
- Müller, M. A., Merten, L. J. F., Böhmer, C., and Nyakatura, J. A. (2021). Pushing the boundary? Testing the “functional elongation hypothesis” of the giraffe’s neck. *Evolution* 75, 641–655. doi: 10.1111/evo.14171
- Nyakatura, J. A., Allen, V. R., Laustroer, J., Andikfar, A., Danczak, M., Ullrich, H.-J., et al. (2015). A three-dimensional skeletal reconstruction of the stem amniote *Orobates pabsti* (Diadectidae): analyses of body mass, centre of mass position, and joint mobility. *PLoS One* 10:e0137284. doi: 10.1371/journal.pone.0137284
- Ogihara, N., Nakatsukasa, M., Nakano, Y., and Ishida, H. (2006). Computerized restoration of nonhomogeneous deformation of a fossil cranium based on bilateral symmetry. *Am. J. Phys. Anthropol.* 130, 1–9. doi: 10.1002/ajpa.20332
- Padian, K., and Chiappe, L. M. (1998). The origin and early evolution of birds. *Biol. Rev.* 73, 1–42. doi: 10.1111/j.1469-185X.1997.tb00024.x
- Pintore, R., Delapré, A., Lefebvre, R., Botton-Divet, L., Houssaye, A., and Cornette, R. (2022). The potential and limits of *Thin-Plate Spline* retrodeformation on asymmetrical objects: simulation of taphonomic deformation and application on a fossil sample of limb long bones. *C. R. Palevol* 21, 191–205. doi: 10.5852/cr-palevol2022v21a9
- Piras, P., Profico, A., Pandolfi, L., Raia, P., Di Vincenzo, F., Mondanaro, A., et al. (2020). Current options for visualization of local deformation in modern shape analysis applied to paleobiological case studies. *Front. Earth Sci.* 8:66. doi: 10.3389/feart.2020.00066
- Ponce De León, M. S., and Zollikofer, C. P. E. (1999). New evidence from Le Moustier 1: computer-assisted reconstruction and morphometry of the skull. *Anat. Record* 254, 474–489. doi: 10.1002/(sici)1097-0185(19990401)254:4<474::aid-aid3>3.co;2-v
- Porro, L. B., Rayfield, E. J., and Clack, J. A. (2015). Descriptive anatomy and three-dimensional reconstruction of the skull of the early tetrapod *Acanthostega gunnari* Jarvik, 1952. *PLoS One* 10:e0118882. doi: 10.1371/journal.pone.0118882
- R Core Team (2019). *R: A Language and Environment for Statistical Computing*. Vienna: R Foundation for Statistical Computing.
- Rahman, I. A., Adcock, K., and Garwood, R. J. (2012). Virtual fossils: a new resource for science communication in paleontology. *Evol. Educ. Outreach* 5, 635–641. doi: 10.1007/s12052-012-0458-2
- Rahman, I. A., and Lautenschlager, S. (2017). Applications of three-dimensional box modeling to palaeontological functional analysis. *Paleontol. Soc. Pap.* 22, 119–132. doi: 10.1017/scs.2017.11
- Rossoni, M., Barsanti, S., Colombo, G., and Guidi, G. (2020). Retopology and simplification of reality-based models for finite element analysis. *Comput. Aided Design Appl.* 17, 525–546. doi: 10.14733/cadaps.2020.525-546
- Schlager, S., Profico, A., Di Vincenzo, F., and Manzi, G. (2018). Retrodeformation of fossil specimens based on 3D bilateral semi-landmarks: implementation in the R package “Morpho”. *PLoS One* 13:e0194073. doi: 10.1371/journal.pone.0194073
- Schwarz-Wings, D., Meyer, C. A., Frey, E., Manzi-Steiner, H.-R., and Schumacher, R. (2010). Mechanical implications of pneumatic neck vertebrae in sauropod dinosaurs. *Proc. R. Soc. B Biol. Sci.* 277, 11–17. doi: 10.1098/rspb.2009.1275
- Shubin, N. H., Daeschler, E. B., and Jenkins, F. A. (2006). The pectoral fin of *Tiktaalik roseae* and the origin of the tetrapod limb. *Nature* 440, 764–771. doi: 10.1038/nature04637
- Sorkine, O., Cohen-Or, D., Lipman, Y., Alexa, M., Rössl, C., and Seidel, H.-P. (2004). “Laplacian surface editing,” in *Proceedings of the 2004 Eurographics/ACM SIGGRAPH Symposium on Geometry Processing - SGP '04*, Vol. 71, (New York, NY: Association for Computing Machinery), 175. doi: 10.1145/1057432.1057456
- Tallman, M., Amenta, N., Delson, E., Frost, S. R., Ghosh, D., Klukkert, Z. S., et al. (2014). Evaluation of a new method of fossil retrodeformation by algorithmic symmetrization: crania of Papionins (Primates, Cercopithecidae) as a Test Case. *PLoS One* 9:e100833. doi: 10.1371/journal.pone.0100833
- Thewissen, J. G. M., Williams, E. M., Roe, L. J., and Hussain, S. T. (2001). Skeletons of terrestrial cetaceans and the relationship of whales to artiodactyls. *Nature* 413, 277–281. doi: 10.1038/35095005
- Tschopp, E., and Mateus, O. (2013). The skull and neck of a new flagellicaudatan sauropod from the Morrison Formation and its implication for the evolution and ontogeny of diplodocid dinosaurs. *J. Syst. Palaeontol.* 11, 853–888. doi: 10.1080/14772019.2012.746589
- Tschopp, E., and Mateus, O. (2017). Osteology of *Galeamopus pabsti* sp. nov. (Sauropoda: Diplodocidae), with implications for neurocranial closure timing, and the cervico-dorsal transition in diplodocids. *PeerJ* 5:e3179. doi: 10.7717/peerj.3179
- Tschopp, E., Russo, J., and Dzemski, G. (2013). Retrodeformation as a test for the validity of phylogenetic characters: an example from diplodocid sauropod vertebrae. *Palaeontol. Electron.* 16, 1–23. doi: 10.26879/312
- Vidal, D., and Díez Díaz, V. (2017). Reconstructing hypothetical sauropod tails by means of 3D digitization: *Lirinosaurus astibiae* as case study. *J. Iberian Geol.* 43, 293–305. doi: 10.1007/s41513-017-0022-6
- Wang, X., Grohé, C., Su, D. F., White, S. C., Ji, X., Kelley, J., et al. (2018). A new otter of giant size, *Siamogale melilutra* sp. nov. (Lutrinae: Mustelidae: Carnivora), from the latest Miocene Shuitangba site in north-eastern Yunnan, south-western China, and a total-evidence phylogeny of lutrines. *J. Syst. Palaeontol.* 16, 39–65. doi: 10.1080/14772019.2016.1267666
- Wedel, M. J. (2005). “Postcranial skeletal pneumaticity in sauropods and its implications for mass estimates,” in *The Sauropods: Evolution and Paleobiology*, 1st Edn, eds K. A. Curry Rogers and J. A. Wilson (Berkeley, CA: University of California Press), 201–228. doi: 10.1525/california/9780520246232.003.0008
- White, T. (2003). Early hominids—diversity or distortion? *Science* 299, 1994–1997. doi: 10.1126/science.1078294
- Wilson, J. A. (1999). A nomenclature for vertebral laminae in sauropods and other saurischian dinosaurs. *J. Vertebr. Paleontol.* 19, 639–653. doi: 10.1080/02724634.1999.10011178
- Xu, X., Ma, Q., and Hu, D. (2010). Pre-*Archaeopteryx* coelurosaurian dinosaurs and their implications for understanding avian origins. *Chin. Sci. Bull.* 55, 3971–3977. doi: 10.1007/s11434-010-4150-z
- Yates, A. M., Wedel, M. J., and Bonnan, M. F. (2012). The early evolution of postcranial skeletal pneumaticity in sauropodomorph dinosaurs. *Acta Palaeontol. Pol.* 57, 85–100. doi: 10.4202/app.2010.0075
- Zollikofer, C. P. E., Ponce de León, M. S., Lieberman, D. E., Guy, F., Pilbeam, D., Likius, A., et al. (2005). Virtual cranial reconstruction of *Sahelanthropus tchadensis*. *Nature* 434, 755–759. doi: 10.1038/nature03397

Conflict of Interest: HM owns the company Palaeo3D. He performed all work on this manuscript in his function as an associate researcher at the Zoological Museum of the Universität Hamburg.

The remaining authors declare that the research was conducted in the absence of any commercial or financial relationships that could be construed as a potential conflict of interest.

Publisher’s Note: All claims expressed in this article are solely those of the authors and do not necessarily represent those of their affiliated organizations, or those of the publisher, the editors and the reviewers. Any product that may be evaluated in this article, or claim that may be made by its manufacturer, is not guaranteed or endorsed by the publisher.

Copyright © 2022 Demuth, Benito, Tschopp, Lautenschlager, Mallison, Heeb and Field. This is an open-access article distributed under the terms of the Creative Commons Attribution License (CC BY). The use, distribution or reproduction in other forums is permitted, provided the original author(s) and the copyright owner(s) are credited and that the original publication in this journal is cited, in accordance with accepted academic practice. No use, distribution or reproduction is permitted which does not comply with these terms.